TECHNICAL RISK AS A COST FACTOR IN COAL LIQUEFACTION: SOME FINANCIAL CONSIDERATIONS

David A. Tillman

Senior Fuel Scientist
Envirosphere Co.
Bellevue, Washington

INTRODUCTION

The U. S. economy is fueled largely by liquid fuels obtained, in no small measure, from unstable sources. The litany of wars, embargoes, and sudden price hikes implies that developing alternative indigenous supplies of liquid fuel is a national economic security issue. Liquid fuels derived from coal are among the alternatives available.

Coal liquids must replace petroleum products in existing applications when they enter the marketplace. That point of entry is almost unique [1-3]. Coal liquids must replace oil directly, for domestic oil supplies are declining. This is also unique in the energy supply history of this country [4-5]. Thus the entry of coal liquids into the economy is fraught with uncertainties caused by unusual conditions.

Uncertainties in the marketplace exist; however a technical base for the development of a coal liquids industry has been developed. Generically four approaches have been pursued: pyrolysis, solvent extraction, catalytic hydrogenation, and indirect liquefaction. Of these, indirect liquefaction is being practiced commercially in countries outside the United States [6].

The existence of a technical base does not imply that coal liquefaction is a mature technology. Rather, it shows that there is a significant gap between what is technologically available and what is economically available. This gap can be attributed to the efficiencies, the capital costs, and the financial risks of such systems. Those financial risks are substantially influenced by the magnitude of the investments and the status of the technology.

This financial gap has not always been recognized in the literature. In order to show the influence of this risk-related issue on coal liquefaction costs and market potentials, the following

considerations are addressed here: (1) a review of previous cost estimating practices, (2) an evaluation of U.S. investment practice related to innovative processes, and (3) the influence of those factors on the costs of coal liquids.

In 1976 a major coal liquids economics symposium was held by the American Chemical Society. In this symposium a common set of economic assumptions were employed. The 1976 ACS symposium, and the values in Table 1 used in that meeting, represents a major step in unifying coal liquefaction economics. However these assumptions do not lead to a solid financial analysis of coal liquefaction plants, and for the following reasons: (1) they intertwine the "what to finance" with "how to finance" decisions; (2) they mask the fact that cash flow, not profit, supports a corporation; and (3) they do not incorporate the influence of technical risk into the discount rate.

The first defect argues that corporations will view new technologies with the same investment ground rules as existing technologies. Corporations are risk averse, however, and prefer to invest in improved existing systems rather than higher risk new systems [8]. Higher rates of discount are required to attract capital into new projects. The second and third deficiencies are violations of the principles of financial analysis [10]. The use of any or all of these three assumptions leads to overly optimistic product cost values.

Given these problems, it is useful to reexamine the discount rate used in calculating coal liquid costs, adjust the accounting procedures to separate "what to finance" from "how to finance," and analyze costs in a way to maximize cash flow. With these adjustments, order of magnitude price estimates may be made and, more importantly, the influences of risk and experience on product costs can be made.

THE DISCOUNT RATE AND COAL LIQUID COSTS

The nominal discount rate is composed of three elements as shown in formula (1):

$$DR = I + M + R \tag{1}$$

Where I = the inflation rate, M = the riskless cost of money (sometimes referred to as the premium for early availability of funds), and R = the premium for total investment risk [10]. Risk can be broken down further into several components as shown in formula (2):

$$R = f(R_e, R_b, R_f, R_t) \tag{2}$$

Where R_e = economic risk (e.g., the risk of a recession), R_b = business

risk, R_f = financial risk (e.g., degree of leverage) and R_t = technological risk. For most firms, the R_e term is uncontrollable and is not isolated. R_t is usually subsumed in business risk if no major innovation is contemplated, where the major innovation will influence the capital structure.

Calculating the Discount Rate

Each major industry has its own appropriate nominal discount rate reflecting the financial investments of debt and equity participants in that industry. While several models exist for calculating the discount rate, the Modiglani-Miller (M-M) theorem is sufficient for these purposes. The model is shown in equation (3) from Haley and Schall [11].

$$DR = \theta K_d + (1 - \theta) K_e \tag{3}$$

Where θ = the proportion of debt, K_d = the cost of debt (including tax effects) and K_e = the cost of equity capital. K_d is taken as the yield-to-maturity on bonds multiplied by 1-TR where TR = the Tax Rate, fractional basis. K_e can be calculated by several techniques varying in sophistication. Again, due to the imprecise nature of discount rate estimation in the face of technological risk, the simplistic approach is taken here and shown in formula (4).

$$K_e = D/P + G \tag{4}$$

Where D = expected dividends, P = stock price, and G = the expected growth rate of the (stock) investment over its useful life.

The M-M model applies to traditional investments and is based upon the principle that, while increasing the debt fraction decreases the apparent discount rate, it increases the degree of leverage, the financial risk and hence the cost of equity capital. Based upon the above equations, Tables 2 and 3 are presented, giving the estimated discount rates for Gulf, Exxon, and Mobil Oil. Growth estimates are based on 10-year earnings/share ratios. For subsequent analysis, the nominal rate of 15% is used since it shows the approximate 1:3 debt/equity ratio common to the energy industry [12] and is the median case calculated.

Table 2 presents the capital structure for Exxon, Gulf, and Mobil--the three companies chosen to develop the discount rate for this industry. Significant is the absence of preferred stock in these companies. Also significant to note is that there is heavy reliance on common stock. Thus the growth issue arises; and it is

complicated by varying expectations concerning the decontrol of petroleum prices.

The Influence of Risk on the Discount Rate

The financial literature is replete with citations concerning the influence of business and financial risk on the discount rate. The typical relationship shown is essentially linear and is referred to as the "Security Market Line" shown in Fig. 1.

Technical risk and/or uncertainty is less well-treated in the literature than busines/financial risk. Technical risk, however, is critical to new energy investment evaluation [13]. Its influence can be evaluated by analogy to traditional business/financial risk assessments.

Empirical studies have addressed the risk issue, including reports by technical Micro Economic Associates [14] and Robert R. Nathan Associates [15]. The former deals largely with the influence of risks on supplies and prices; and the latter shows rates of return obtained on innovations in U.S. industry since 1940. Pre-tax private internal rates of return (IRR) ranged from negative to 157% over a broad spectrum innovations on a real dollar basis.

Two petroleum industry innovations, one in extraction and one in processing, showed pre-tax IRR values of 50 to 56% in the Nathan Associates study. This is slightly higher than the median value of 34 to 38%. Given standard economic assumptions, after tax rates of return can be calculated at ∿20% on average and ∿30% in the petroleum industry. It should be noted that the petroleum related investments were made in 1942 and 1949. However, a mining related innovation introduced in 1964 had a pre-tax IRR of 54%. These IRR values are not discount rates per se, but they give some clue to investor expectations. Thus, resource industry innovations may generally require the higher discount rates.

The risk-adjusted discount rate also is a function of some learning curve concerning the new technology. Those extractive industry innovations which first earned ∿30% after taxes now require ∿15%. The initial parts of the investment learning curve, both technically and financially, relate to the process of going from concept development and bench scale research to commercial technologies through process development units and then pilot plants. Swabb [16] identifies the preferred succeeding step from pilot plant to commercial technology as a pioneer plant, to be owned and operated by the private industry as a commercial facility followed by the design and construction of succeeding commercial plants. The pioneer plant

is critical in this approach as it demonstrates plant reliability, product output, environmental protection safeguards, and commercial viability. It reduces business risk to manageable levels.

If one accepts the Schwabb argument, then the discount rate for the pioneer plant may be nominally ∿30%. The lower limit is, of course, nominally 15%. The upper limit, however, remains essentially undefined. Further, the number of commercial plants required to go from 30% to 15%, is also undefined.

Similar learning curves have been posited for capital cost estimates [17, 18]. Such curves take the form of sensitivity analysis parameters. The analogy between capital cost and discount rate estimation is imperfect, both sets of data deal with investment uncertainties as perceived by boards of directors. Despite these uncertainties, a 30% discount rate is used here for pioneer plants, and a 15% discount rate is used for mature plants.

The empirical technical risk adjustment made here is analogous to an unusual business risk taken. Before the passage of the Public Utility Regulatory and Policies Act (PURPA), industries entering cogeneration ventures perceived the following risks: (1) would they be regulated as utilities; (2) would utilities purchase surplus power from them; and (3) would utilities sell them power as needed at a reasonable cost. Frequently after-tax rates of return demanded by cogenerators were 30% [19]. Again it is an imperfect analogy. The investment community is consistent--manufacturing industry. The broad investment arena is energy. The cogeneration technology, however, is mature. Thus this risk adjustment is only one more indicator of investor behavior.

CALCULATED COSTS OF COAL LIQUIDS UNDER UNUSUAL AND NORMAL RISK CONDITIONS

Remaining are the tasks of estimating the initial costs of coal liquids and the price reductions possible as investor corporations gain commercial experience in coal liquefaction. Accomplishing these evaluations requires making some accounting assumptions. It then involves calculating fuel costs based on the systems selected.

Accounting Conventions and Assumptions

In the projecting of synthetic fuel costs, certain conventions play an important role: (1) the selection of a depreciation method; and (2) the selection of a dollar basis.

Three depreciation methods exist: straight line, sum-of-the years digits, and double declining balance. In general, the latter two accelerated systems generate more favorable cash flows (depending upon the capital strucutre of the industry). The double declining balance method generates particularly high depreciation values in the first few years. Thus, it is used here.

Depreciation may be taken over a variety of time periods. To maximize cash flow, and the contribution of depreciation to net present value, the shortest possible depreciation period is preferred. The Internal Revenue Service [20] gives a minimum of 13 years for petroleum refineries; and this value is assumed to hold for coal liquefaction plants.

Depreciation is the major area of capital recovery meriting documentation. Historical statistics can be used to develop assumptions for cost increases over time. These are shown in Table 4. These values are used in constructing proforma statements.

System and Product Costs

Two systems have been selected for analysis here: (1) methanol synthesis and (2) solvent extraction. Methanol is advanced frequently as a technology of immediate application [21, 22]. Solvent extraction is considered one of the leading candidates for boiler fuels production [23]. Both systems are described generically in Sliepcevich et al. [24]. Table 5 presents the significant capital cost and product output parameters for each unit. The cost values have been updated to 1980 dollars from the original publication by use of the chemical engineering plant cost index as reported in the Engineering News Record [25].

Both the methanol and solvent extraction plants were estimated to cost $\$1 \times 10^9$ in 1977, and are now estimated to cost $\$1.3 \times 10^9$. After removal of the 20% investment tax credit, these capital costs are $\$1.04 \times 10^9$. If one assumes a 13-year amortization period, the risky investment with a discount rate of 30% must generate an annual after-tax cash flow of $\$322 \times 10^6$. If the technology were considered by investors to be mature, that after-tax cash flow requirement would be $\$178 \times 10^6$. The differential is particularly significant since investment tax credits and depreciation are calculated without regard to technological matury. Thus the $\$144 \times 10^6$ must be made up entirely with after-tax profits.

From these data, modified proforma statements have been constructed for both technologies assuming: (1) instantaneous construction and startup and (2) constant after-tax cash flows. These

are optimistic assumptions but they do not affect the analysis of financial risk reduction seriously, since they are constant relative to the variable discount rate. Table 6 is the proforma statement for selected years of the risky solvent extraction plant. Table 7 is the proforma statement for the same years assuming a mature technology. Values are in nominal (inflated) dollars.

It is significant to note that the high risk plant must be profitable from the start. The mature plant can sustain losses during the first year without jeopardizing the cash flow stream. Depreciation is for more significant to the mature plant than the high risk pioneer plant. Similar proforma statements can be constructed for methanol plants. Revenue streams can then de deflated to 1980 dollars by the following formula:

$$D_t = 1.064^t \qquad (8)$$

Where D = deflator and t = the year of operation. From these values Table 8 is constructed showing the approximate cost of fuels from pioneer plants and mature plants. In both cases the gaining of financial experience carries a cost savings of about $10/bbl of oil equivalent.

What is significant here is not the $40/bbl or $60/bbl value. These are best guesses based upon available information from pilot plants. Nobody knows what coal liquids will actually cost. Rather, it is the cost reduction associated with investor experience which is significant. Cost savings of $1-2/10^6 Btu are substantial. These result from a reduction in the discount rate as risks and uncertainties are reduced.

CONCLUSION

Substantial fuel cost savings, then, are available from corporation investment experience in coal liquefaction facilities. These savings are in the vicinity of $10/bbl or $1-2/10^6 Btu. These savings also should be pursued. These substantial price reductions may be achieved when investors advance along their own learning curve. That learning curve equates the relationship of expected product price and plant performance to achieved product price and plant performance; and translates that relationship plus market acceptance of the product into a risk factor and an appropriate discount rate. Large savings in fuel costs can be achieved only when investors have advanced sufficiently to reduce their perceptions of liquefaction risk and uncertainty.

REFERENCES

1. Hottel, H. C. and J. B. Howard. 1971. New Energy Technology: Some Facts and Assessments. MIT Press, Cambridge, Mass.

2. Frey, J. W. and H. C. Ide. 1946. A History of the Petroleum Administration for War: 1941-1945. U.S. Government Printing Office, Washington, D.C.

3. National Materials Advisory Board. 1975. Problems and Legislative Opportunities in the Basic Materials Industry. National Academy of Sciences, Washington, D.C.

4. Tillman, D. A. 1978. Wood as an Energy Resource. Academic Press, New York.

5. Enger, H., W. Dupree, and S. Miller. 1975. Energy Perspectives: A presentation of major energy and energy-related data. U.S. Department of the Interior, Washington, D.C.

6. Smith, I. H. and G. J. Werner. 1976. Coal Conversion Technology. Noyes Data Corp., Park Ridge, N.J.

7. Pelofsky, A. H. 1977. Preface, in Synthetic Fuels Processing: Comparative Economics (Pelofsky, A. H. ed.), Marcel Dekker, New York, iii-v.

8. Perry, H. 1979. Synthetic Fuels Commercialization Testimony before the House Committee on Science and Technology, Sept. 12.

9. Bierman, H., and S. Smidt. 1971. The Capital Budgeting Decision. Macmillan, New York.

10. Schall, L. D., and C. W. Haley. 1977. Introduction to Financial Management. McGraw-Hill, New York.

11. Haley, C. W., and L. D. Schall. 1979. The Theory of Financial Decisions. McGraw-Hill, New York.

12. Haas, J. E., E. J. Mitchell, and B. K. Stone. 1974. Financing the Energy Industry. Ballinger, Cambridge, Mass.

13. Tillman, D. A. 1980. A financial analysis of silvicultural fuel farms on marginal lands. Ph.D. Dissertation, College of Forest Resources, University of Washington, Seattle, Wash.

14. Microeconomic Associates. 1978. Effect of Risk on Prices and Quantities of Energy Supplies. Electric Power Research Institute, Palo Alto, Calif.

15. Robert R. Nathan Assoc. 1978. Net Rates of Return on Innovations: Final Report. Vol. 1. Technical Report. Washington, D.C. (for the National Science Foundation).

16. Swabb, L. E. 1978. Liquid Fuels from Coal: From R & D to an Industry. Science 199(4329), 619-622.

17. Adams, M. R., C. W. Knudsen, and C. W. Draffin. 1977. Economic Evaluation by ERDA of Alternative Fossil Energy Technologies, in Synthetic Fuels Processing: Comparative Economics (Pelofsky, A. H., ed). Marcel Dekker, New York.

18. Beath, B. C. 1979. Guidelines for Economic Evaluation of Coal Conversion Processes. The Engineering Societies Commission on Energy, Washington, D.C.

19. Stobaugh, R. and D. Yergin (eds.). 1979. Energy Future: Report of the Energy Project at the Harvard Business School. Random House, New York.

20. Internal Revenue Service. 1977. Tax Information on Depreciation. Department of the Treasury, Washington, D.C.

21. Perry, H. 1978. Clean fuels from coal, in Advances in Energy Systems and Technologies, Vol. 1 (Auer, P., ed.), Academic Press, New York.

22. Stokes, C. A. 1979. Synthetic Fuels at the Crossroads. Technology Review, Aug/Sept. 25-33.

23. Whitaker, R. 1978. Scaling up coal liquids. EPRI Journal 3 (7) 6-13.

24. Sliepcevich, C. M. et al. 1977. Assessment of Technology for the Liquefaction of Coal. National Research Council/National Academy of Sciences, Washington, D.C.

25. Anon. 1980. Builders' construction cost indexes. Engineering News Record 205(25):77.

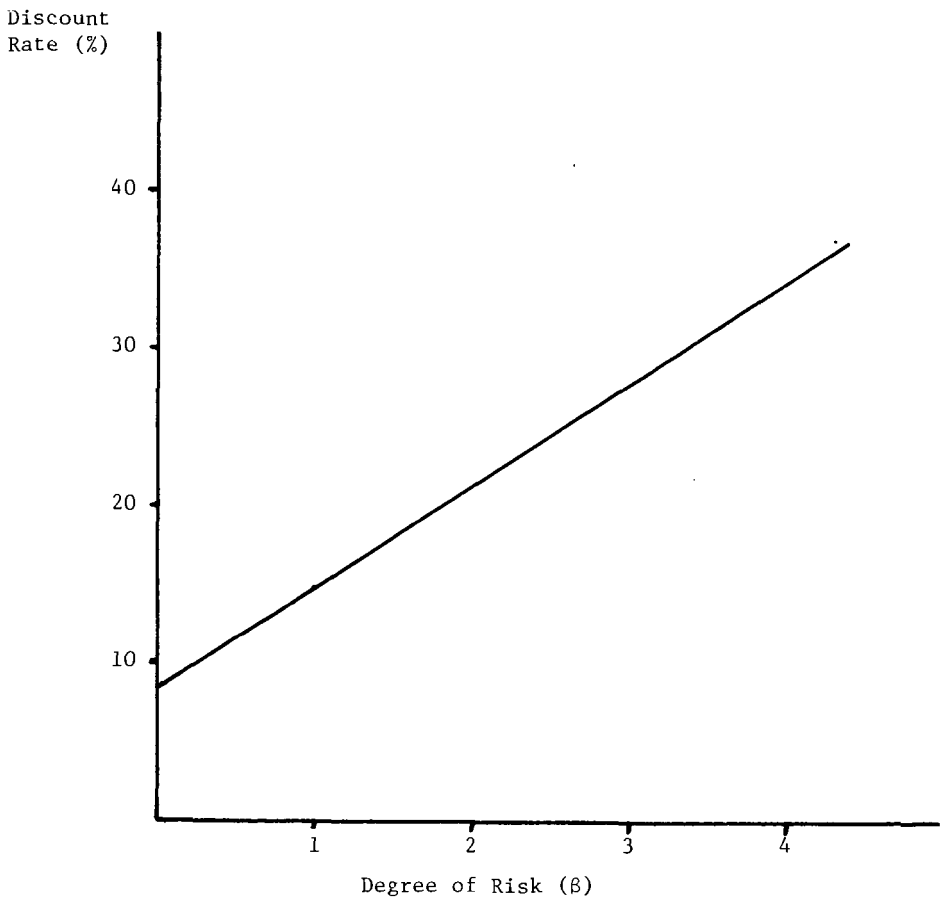

Figure 1. The discount rate, or cost of money, as a function of the degree of risk associated with the investment. This curve is known as the Security Market Line.

TABLE 1. Financial Assumptions for the 1976 American Chemical Society Meeting on Synthetic Fuel Economics

Parameter	Value
Project life	20 years
Cost of capital	10 percent
Depreciation	Straight line
Base Return on Investment[a]	15 percent

[a]Not specified but requently used.
Source: [7]

TABLE 2. The Capital Structure of Three Petroleum Companies, 1979

	Company		
Capital Instrument	Gulf	Exxon	Mobil
Debt	.191	.112	.261
Preferred stock	-0-	-0-	-0-
Common stock	.809	.888	.739
Total	1.00	1.00	1.00

TABLE 3. The Cost of Capital for Three Petroleum Companies (in %)

	Capital Cost Contribution by Company		
Capital Instrument	Gulf	Exxon	Mobil
Debt portion	0.97[a]	0.54[b]	1.18[c]
Common equity portion	11.6 [d]	16.3 [e]	14.0 [f]
Total	12.6	16.8	15.2

[a] .191 x .570 x .089 x 100 = 0.97; .089 = Yield to Maturity on bonds.
[b] .112 x .553 x .087 x 100 = 0.54; .087 = Yield to Maturity on bonds.
(Continued next page.)

[c] .261 x .524 x .086 x 100 = 1.18; 0.86 = Yield to Maturity on bonds.

Second term in all above calculations = 1 - TR for domestic operations. Thus the tax effect of interest is accounted for in the discount rate calculation.

[d] $\frac{2.05}{30.75}$ + .076 = .143; .143 x .809 = .116

[e] $\frac{4}{56.5}$ + .112 = .183; .183 x .888 = .163

[f] $\frac{2.40}{42.625}$ + .135 = .190; .190 x .739 = 14.0

General formula for d, e, f, is $\frac{D_e}{P_e} + G = K_{ceq}$ as defined as follows:

The cost of common equity capital is determined by $D_e/P + G_e = K_{ceq}$ where D_e = expected dividend, P = price, and G_e = expected growth and K_{ceq} = capital cost, common equity.

Sources: Annual Reports, 1978; Standard and Poor's Bond Guide, August, 1979; WSJ, August 28; Value Line.

TABLE 4. Real Price Increases 1968-1978

Good/Service	10 Yr Nominal Rate (%)	10 Yr Real Rate (%)
All goods and Services (CPI)	6.4	-0-
Labor		
Utilities	8.4	2.0
Chemical manufacturing	8.3	1.9
Fuels and Energy		
Coal	11.7	5.3
Electricity	9.3	2.9
Supplies		
Chemicals (Industrial)	8.3	1.9
Miscellaneous supplies	6.0	-0.4
Services	7.0	0.6

Sources: U. S. Census Bureau, 1978; U.S. Census Bureau, 1974; U.S. Bureau of Labor Statistics, 1980.

TABLE 5. Cost and Output Parameters for Selected Solvent Extraction and Methanol Plants

Parameter	Technology	
	Solvent extraction	Methanol
Plant size	50×10^3 bbl/day 325×10^9 Btu/day	11,300 tons/day 230×10^9 Btu/day
Thermal efficiency	64%	46%
1977 capital cost total	\$0.9 - 1.15 x 10^9	\$0.85 - 1.2 x 10^9
1977 capital cost/bbl/day	\$16.5 - 21.5 x 10^3	\$23 - 30 x 10^3
Median 1980 capital cost (gross)	\$1.3 x 10^9	\$1.3 x 10^9
1980 investment tax credit	\$260 x 10^6	\$260 x 10^6

Source: [24].

TABLE 6. Pro Forma Statement for the Solvent Extraction Plant 30% Discount Rate (Values in \$ x 10^6)

Cost/Income Stream	Year		
	1	5	13
Revenue	655	988	1677
Operating cost			
Fuel	223	347	841
Labor	6	8	15
Chemicals and supplies	14	18	31
Water and utilities	2	2	3
Maintenance	68	94	177
Taxes and insurance	16	20	37
Depreciation	200	103	27
Earnings before taxes	226	406	546
Income tax (46%)	104	187	251
Net income after taxes	122	219	295
Depreciation	200	103	27
Cash flow	322	322	322

Sources: Table 5 and [24].

TABLE 7. Pro Forma Statement for the Solvent Extraction Plant - 15% Discount Rate (Values in $ x 10^6)

Cost/Income Stream	Year 1	Year 5	Year 13
Revenue	507	731	1411
Operating cost			
Fuel	223	347	841
Labor	6	8	15
Chemicals and supplies	14	18	31
Water and utilities	2	2	3
Maintenance	68	94	177
Taxes and insurance	16	20	37
Depreciation	200	103	27
Earnings before taxes	(22)	139	280
Income tax (46%)	-0-	64	129
Net income after taxes	(22)	75	151
Depreciation	200	103	27
Cash flow	178	178	178

Sources: Table 5 and [24].

TABLE 8. Levelized Fuel Costs for Pioneer and Mature Coal Conversion Plants (in 1980 Dollars)

Coal Liquefaction System	Fuel Cost: Pioneer Plant $/$10^6$ Btu	Pioneer Plant $/bbl	Mature Plant $/$10^6$ Btu	Mature Plant $/bbl
Solvent extraction	8	50	7	40
Methanol	10	60	8	50

SYNTHETIC POLYMERS AS MODELS FOR COAL IN A DESULFURIZATION PROCESS

Thomas E. Schmidt, Thomas G. Squires and Clifford G. Venier

Ames Laboratory*, Iowa State University, Ames, Iowa 50011

Oxydesulfurization processes use air or oxygen to remove sulfur from coal for the purpose of converting high sulfur coal into an environmentally acceptable solid fuel (1). The desulfurization is mainly from the conversion of pyritic sulfur into sulfate and its removal when the coal is recovered from the aqueous slurry of the process (2). Because evidence for the removal of organic sulfur from coal could revitalize the now dormant status of oxydesulfurization as a method of coal beneficiation, we have been investigating the ability of these processes to degrade organic sulfur functions.

A direct comparison of a coal's organic sulfur content before and after process treatment is fraught with uncertainty due to the confusion in distinguishing the various forms of sulfur in coal (3). Therefore, our evaluation of the Ames Process, which employs oxygen and 0.2 M aqueous sodium carbonate at 200 psi total pressure and 150° C, has been based on the use of model compounds (4). In these investigations, the organic sulfur functional groups exhibited one of three kinds of behavior: direct autoxidation of the sulfur, indirect oxidation of the sulfur via autoxidation of an adjacent, benzylic C-H bond; and no reaction. Thiols and disulfides were directly oxidized to sulfonates which were stable under process conditions (i.e. no carbon-sulfur bond cleavage). Model compounds containing a benzylic sulfide function gave products (Equation 1) via a reaction pathway which is analogous to the autoxidation of benzylic C-H's in diarylmethanes (Equation 2). Other sulfides were recovered unchanged after one hour under Ames Process conditions.

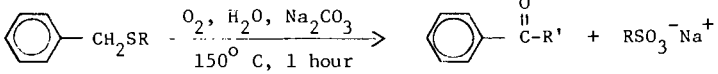

R = methyl or phenyl, R' = H or OH

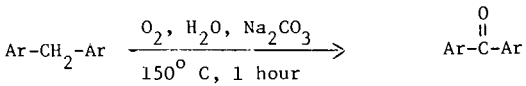

The further evaluation of the Ames Process with model compounds has been aimed at considering the relation between desulfurization and the autoxidative degradation of the substrate as a whole.

The evaluation of oxydesulfurization processes using simple model compounds is well suited for determining the reactivity of particular functional groups, but does not speak to effects on that reactivity when such are part of an extended hydrocarbon matrix. The influence of the proximate environment on the oxidation of sulfur functions is expected to be based on factors such as:

1) inhibition to mass transport of reagents or oxidation products;
2) competitive reactivity by hydrocarbon functions; and
3) intramolecular propagation of autoxidation.

In order to devise a model substrate for process evaluation in which sulfur is incorporated in a hydrocarbon matrix while maintaining the ability to describe the results in terms of functional group reactivity, we have prepared a series of synthetic polymers which meet the requirements outlined below :

---

*Operated for the U.S. Department of Energy by Iowa State University under Contract No. W-7405-Eng-82. This research was supported by the Assistant Secretary for Fossil Energy, Office of Coal Mining, WPAS-AA-75-05-05.

1) a high carbon, hydrogen and sulfur content,
2) a predictable average structure, and
3) sufficient crosslinking to impart insolubility.

Such polymers simulate some of the physical properties of coal and allow the recovery of the hydrocarbon content of the model as a solid product, which procedure is a basis of oxydesulfurization processes.

Materials

The modification, outlined in Figure 1, of chloromethylated polystyrene beads (Biobeads S-X1, 200-400 mesh, BioRad Laboratories, Richmond, CA) provides a convenient entry to several polymers meeting the above requirements as well as being comparable one with another. The preparation of a formaldehyde condensation polymer (Figure 2), which is closer than polystyrene to the H/C ratio of coals and is high in diarylmethane functions, was also carried out although this polymer is less defined as to its average size and structure. Similar condensation polymers, without sulfur, had previously been proposed as models for coal (5).

Experimental

The procedure by which the synthetic polymers were subjected to the Ames Process is described here. The dry polymer, 0.6 to 1.8 g, and 100 ml of 0.2 M aqueous sodium carbonate were placed in a 300 ml autoclave, which was flushed three times with nitrogen at 80 psi pressure, and the sealed autoclave was heated to the operating temperature. When the temperature had reached 150° C, oxygen was added to a total pressure of 200 psi and the autoclave was vented until the pressure was about 100 psi. The addition of oxygen was repeated twice, then the sealed autoclave was stirred at 1500 rpm for 1 h. while maintaining the temperature at 150 $\pm$ 10° C. In the case of these polymers, no significant amount of material was lost by the venting procedure. After cooling to room temperature the residual pressure (70 to 90 psi) was vented. The solid was collected by filtration, using 400 ml of distilled water to rinse the autoclave and wash the solid. The solid was successively washed with 30 ml portions of methanol, THF and benzene, then dried under reduced pressure and 80 to 90° C for at least five h. prior to weighing, recording the IR spectrum (KBr pellet) and submitting a sample for elemental analysis (elemental analyses were performed by Galbraith Laboratories, Knoxville, TN). The residue obtained by evaporation of the combined organic solvents exhibited PMR and IR spectra characteristic of polystyrene. In the case of (4-polystyryl)methyl 4-tolyl sulfide (1), sodium 4-toluenesulfonate in the residue of the aqueous phase was measured by its integral intensities in the PMR spectrum relative to t-BuOH as an internal standard. In the case of benzyl (4-polystyryl) sulfide (2), the aqueous phase was extracted with dichloromethane and benzaldehyde was found to be present in the extract in a yield of 19 % based on the amount of sulfur in 2.

Results

The effect of the Ames Process on the synthetic polymers was monitored by the degree of solubilization and the elemental analysis of the solid product. For polystyrenes, the formation of soluble polymers is a measure of the extent of autoxidation of the polystyryl backbone (6); this degradation will have no significant effect on the S/C ratio of the recovered solids. It is only when a C-S bond is more susceptible to autoxidative cleavage than the polymer backbone that a marked change in the S/C ratio can occur. This behavior is exhibited by polymers 1 (Table 1) and 2 (Table 2) which contain the benzylic sulfide function. The decrease in the S/C ratio in recovered polymer 1 and the increase in this ratio for recovered polymer 2 is explained by the facile autoxidation reactions shown in Equations 3 and 4.

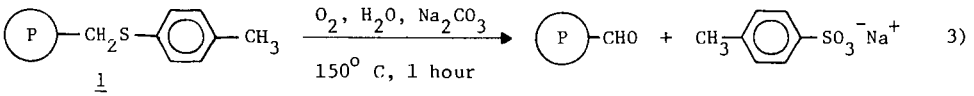

1 3)

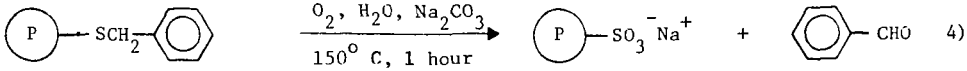

2

While the extent of desulfurization and polymer solubilization of 1 over four seemingly identical runs (Table 1) were quite variable, there is a correlation between the two types of degradation, i.e. more desulfurization was accompanied by more solubilization. That radical initiation of autoxidation is important for both processes was shown by the fact that the inclusion of a specific initiator, 2,2'-azobis (2-methylpropionitrile) (AIBN), increased both desulfurization and solubilization of polymer 1. In contrast, the use of AIBN with 7 was counter-productive with respect to desulfurization. This result is entirely consistent with our earlier findings that DBT is inert to Ames Process conditions and with our postulate that C-S bond cleavage must be initiated by autoxidation of an α-H.

When coal is subjected to an oxydesulfurization process, indigenous labile functions can presumably initiate autoxidation. It has been reported for example, that the pyridine soluble portion of coal contains substances which promote the air oxidation of coal at 100° C (7). To test whether a pyridine extract of coal could initiate the autoxidation of 1, we added such an extract to 1 under the conditions of the Ames Process. This result is reported in Table 1 and leads to the conclusion that the extract was not an effective initiator of autoxidation under these conditions.

Table 2 contains sulfur functions which are inert to the process conditions, i.e. DBT, $DBTO_2$ and ethyl phenyl sulfone; and, in these systems, autoxidation was not accompanied by desulfurization. This is especially evident with the condensation polymer 7, which is perhaps a better model for coal than polystyrene (8). The ability of the Ames Process to oxidize fluorene (4) suggested that 7 should undergo autoxidation. This was established on the basis of the degree of solubilization, the presence of carbonyl functions in the recovered solid (as detected by IR, 1715 cm^{-1}) and the incorporation of oxygen in the solid.

Conclusions

Although the Ames Process was designed to oxidize and remove sulfur from coal, these reaction conditions promote autoxidation of hydrocarbon functions as well, and the relative rates of hydrocarbon oxidation and organic sulfur removal are determined by the particular structure of each. Benzylic sulfides were the only case examined where C-S bond cleavage was significant precisely because of its greater susceptibility to autoxidation relative to the hydrocarbon part of the polymer. When incorporated into a hydrocarbon polymer, benzylic sulfides were found to be less reactive under the process conditions than the monomer benzyl phenyl sulfide (4). There is no indication that the hydroperoxides, which are formed by autoxidation of labile C-H bonds, react with sulfides to produce sulfoxides or sulfones under these conditions.

In this evaluation of the Ames Process with polymer models, we have shown that:

1) only benzylic sulfides undergo preferential C-S bond cleavage;

2) this cleavage is a radical process analogous to hydrocarbon autoxidation;

3) conditions which accelerate the oxidative cleavage of these C-S bonds will also increase the rate of degradation of the hydrocarbon matrix;

4) as expected, the rate of reaction of the benzylic C-S bond is attenuated when the sulfide is incorporated into an insoluble polymer.

Figure 1. Synthesis of Modified Polystyrenes for Use as Coal Models.

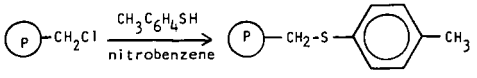

1: 83.59 %C, 7.09 %H, 8.87 %S, 0.23 %Cl

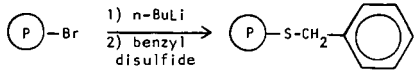

2: 83.24 %C, 7.11 %H, 8.40 %S, 1.12 %Br

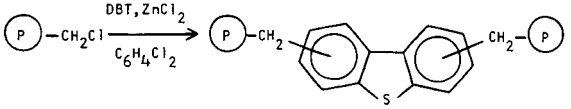

3: 87.59 %C, 6.82 %H, 4.58 %S

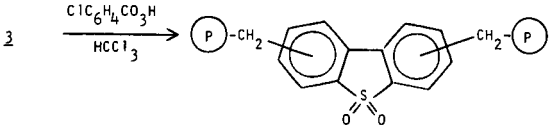

4: 83.78 %C, 6.61 %H, 4.44 % S

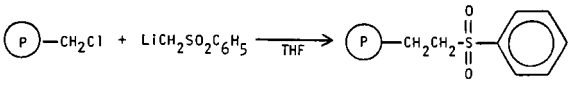

5: 80.82 %C, 7.25 %H, 5.84 %S

Figure 2. Hypothetical Structure for DBT/Fluorene/Formaldehyde Copolymer (7).

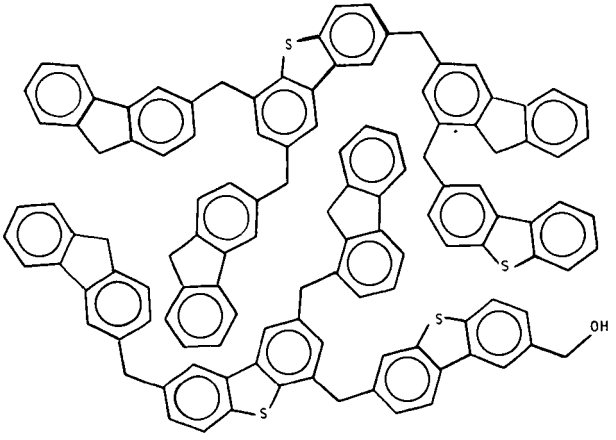

7: 86.72 %C, 5.01 %H, 7.75 %S

TABLE 1. Effect of Ames Process on (4-Polystyryl)methyl 4-Tolyl Sulfide (1).[a]

Initial Wgt.	Recovered as a Solid[b]				% CH_2-S[c]	4-Tolyl	Soluble[d]
	Weight	Carbon	Sulfur	ΔS/C	Cleavage	Sulfonate	Polymer
0.91 g	84 %	81 %	57 %	-30 %	37 %	22 %	4.5 %
0.91	92	90	76	-16	21	28	2.7
1.14	93	91	76	-17	22	18	1.7
0.60	92	93	92	- 1	2	0.3	0
average of four	90	89	75	-16	20	17	2.2
1.00[e]	89	88	76	-13	17		-
0.74[f]	86	83	54	-34	42		9.3

TABLE 2. Effect of Ames Process on Some Synthetic Polymers.[a]

Polymer	Initial Wgt.	Recovered as a Solid[b]				Soluble[d]
		Weight	Carbon	Sulfur	ΔS/C	Polymer
Polystyrene[g]	1.59 g	96 %	96 %	-	-	2.3 %
Polystyrene[g,h]	1.50	95	-	-	-	0.7
2	0.62	87	84	98 %	+17 %	3.2
3	0.78	96	96	97	+ 1	1.4
4	0.73	104	101	102	+ 1	1.0
5	1.16	94	95	96	+ 1½	0
7	1.06	89	87	88	+ 2	9.4
7[f]	0.90	95	92	95	+ 5	4.0

a) See Figures 1 and 2 for the structures of the polymers.
b) Presented as a percentage of the corresponding original values.
c) This is based on the loss of sulfur relative to the polystyryl carbon, which is the total carbon less the carbon due to the 4-tolyl groups, and is calculated as 100 % - 100 % $(S_pC_i - 7S_pS_i) \div (S_iC_p - 7S_pS_i)$ where S_p is the moles per unit weight of sulfur in the solid product, S_i is the moles of sulfur in the initial polymer, C_i is the moles of carbon in the initial polymer and C_p is the moles of carbon in the solid product.
d) Residue after evaporation of the organic solvents as a percentage of the initial weight.
e) Pyridine extract of an Ill. No. 6 coal, 0.1 g, was added to this run; the presence of the extract masked detection of soluble polymer.
f) With 0.16 g of AIBN added and oxygen added before heating the autoclave.
g) Biobeads S-X1, 200-400 mesh, prewashed with benzene and MeOH.
h) N_2 atmosphere only instead of O_2; elemental analysis not obtained.

REFERENCES

1. (a) S. Friedman, R.B. LaCount and R.P. Warzinski, in Coal Desulfurization, T.D. Wheelock, ed., A.C.S. Symposium Series, 64, 164-172 (1977); (b) S. Sareen, ibid., 173-181; (c) C.Y. Tai, G.V. Graves and T.D. Wheelock, ibid., 182-197.
2. T.D. Wheelock, R.T. Greer, R. Markuszewski and R.W. Fisher, Advanced Development of Fine Coal Desulfurization and Recovery Technology, Annual Technical Progress Report, Oct. 1, 1976-Sept. 30, 1977, submitted to the U.S. Department of Energy, Ames Laboratory, Iowa State University, Document No. IS-4363, March, 1978.
3. B. Paris, in Coal Desulfurization, T.D. Wheelock, ed., A.C.S. Symposium Series, 64, 22-31 (1977).
4. T.G. Squires, C.G. Venier, L.W. Chang and T.E. Schmidt, ACS Div. Fuel Chem., PREPRINTS, 26, No. 1, 50-55 (1981).
5. (a) P. Wolfs, D. Van Krevelen and H. Waterman, Brennstoff-Chemie, 40, 215-222, (1959); (b) L. Lazrov and S. Angelov, Fuel, 59, 55-58 (1979).
6. L. Dulog and K.-H. David, Die Makromolekulare Chemie, 145, 67-85 (1971).
7. V.A. Sukhov, et.al., Solid Fuel Chemistry (trans. of Khim. Tverd. Topl.), 10, (3), 96-100 (1976).
8. K.-D. Gundermann, G. Fledler and I. Knoppel, Brennstoff-Chemie, 29, 23-27 (1976).

PRODUCT YIELD AND HYDROGEN CONSUMPTION SELECTIVITY TESTS FOR COAL LIQUEFACTION CATALYST DEVELOPMENT*

H. P. Stephens

Sandia National Laboratories, Albuquerque, New Mexico 87185

INTRODUCTION

Because hydrogenation of coal to liquid products (oils) is accompanied by distributions of complex by-product mixtures (IOM, preasphaltenes, asphaltenes and gases) which change as a function of reaction variables (time, temperature and pressure) and reactor configuration, the determination of selectivity relationships for coal liquefaction catalysts has been a difficult and time-consuming task involving numerous experiments to adequately describe catalyst performance over a range of conditions. This paper describes a method for analyzing the experimental results of coal liquefaction reactions which may be applied to a number of aspects of coal liquefaction research and process control, including: rapid selectivity and performance screening for catalysts; correlation of laboratory results with process parameters; and optimization of product yield for plant process conditions. Catalyst selectivity and performance screening will be emphasized here.

A primary goal of catalyst development for direct coal liquefaction is to maximize the yield of distillate products while minimizing the conversion to by-product hydrocarbon gases which unprofitably consume much of the hydrogen. Selectivity relationships for direct coal liquefaction catalysts have been difficult to determine and accurately describe, not only because of the complexity of the reaction mixtures, but also because of the difficulty of comparing the results of experiments performed at different times and temperatures or with different types of reactors. Imprecision in control of experimental variables such as temperature and contact time often causes significant differences in conversions for experiments for which the mean variables were designed to be nominally the same. Thus selectivity comparisons based on conversions at constant time and temperature are not entirely reliable.

The approach to selectivity relationships described in this paper is based on 1) a ternary product distribution diagram with a hyperbolic relation

$$y = \frac{x(c-x)}{a+bx} \qquad 1)$$

between product and by-product conversions and 2) a hydrogen consumption diagram which relates the product conversion to the fraction of hydrogen consumed by the production of hydrocarbon gases. Each of these diagrams correlates, on a single curve, product distributions from reactions carried out over a wide range of experimental parameters, including temperature, time and different reactors.

Waterman first used ternary product distribution diagrams with reaction paths represented by

$$y = \frac{x(1-x)}{a+bx} \qquad 2)$$

* This work supported by the U.S. Department of Energy.

to describe the catalytic hydroisomerization of paraffin wax (1) and later demonstrated their application to the characterization of many other complex chemical processes (2). Although the technique has been used to describe other hydrogenation processes (2,3), application to direct coal liquefaction has been unexplored. The results and analysis of direct coal liquefaction experiments described in this paper demonstrate the general applicability of ternary and hydrogen consumption diagrams to selectivity tests for coal liquefaction catalyst development.

EXPERIMENTAL

Materials

Liquefaction reactions were performed with Illinois No. 6 coal, SRC-II heavy distillate from the Ft. Lewis pilot plant (1:2 coal:solvent, by weight) and high purity hydrogen. An extensively used commercial HDS catalyst, American Cyanamid 1442A, an alumina supported CoMo formulation, was tested to establish base-line selectivity relationships. The catalyst extrudates were ground to a -200 mesh powder and added to the reaction feed slurry on a 5 weight percent coal basis. This quantity of CoMo/alumina was equivalent to 0.15% Co and 0.45% Mo. To test the utility of the selectivity relationships, additional microreactor experiments were performed with 0.3% Mo as molybdenum naphthenate (6% solution of molybdenum in naphthenic acid, obtained from Research Organic/Research Inorganic, Inc.), along with a control experiment with the equivalent amount of naphthenic acid alone.

Apparatus and Procedure

Two types of reactor systems were utilized, 30 cm^3 batch microreactors (4), and a one-liter autoclave (5). For the low to moderate conversion range, microreactor experiments were performed at 1000 psig cold charge hydrogen pressure and over a wide range of times, t = 0.5 to 80 min, and temperatures, T = 350° to 425°C. Two autoclave experiments were conducted at 1000 psig and 425°C for 30 and 120 min to obtain data for high conversions. Temperatures and pressures were accurately recorded during the course of each experiment. Following the heating period of each experiment, the reaction vessel was quenched to ambient temperature, the resulting pressure was recorded, a gas sample was taken, and the product slurry was quantitatively transferred to a flask and subsampled for analysis.

Product Analysis

Gas samples were analyzed for mole percentages of CO, CO_2, H_2S and C_1-C_4 hydrocarbons with a Hewlett-Packard 5710A gas chromatograph, which was calibrated with standard mixtures of hydrocarbon gases and H_2S in hydrogen, obtained from Matheson Gas Products. Hydrogen in the samples was obtained by difference as the remainder of the product gas mixture. The quantity of each gas produced was calculated from the mole percent in the gas sample and the post-reaction vessel temperature T and pressure P using an ideal gas law calculation:

$$n_i = \frac{PV}{RT} f_i \qquad 3)$$

$$w_i = FW_i \, n_i \qquad 4)$$

where n_i = number of moles of component i

f_i = mole fraction of i in the gas sample = mole %/100

V = gas volume of reactor

w_i = weight of i

FW_i = the formula weight of i

Hydrogen consumed during the reaction was obtained as the difference between the initial charge and hydrogen remaining after the reactor was quenched.

The reaction product slurry was analyzed for insols, preasphaltenes, asphaltenes, and oils by tetrahydrofuran (THF) solubility and high performance liquid chromatography (HPLC). A 0.2 gm subsample was mixed with about 50 ml of THF, filtered to obtain the weight of insols, and brought to 100 ml with additional THF. Chromatograms of 5 µl aliquots of the filtrate were obtained with a Waters Assoc. Model 6000A solvent delivery system equipped with a Model 440 uv absorbance detector. Separations of the solution into three fractions, preasphaltenes, asphaltenes, and oils, were effected on 100 A microsyragel gel permeation columns. The uv absorbance response factors for the product separations were determined using standards prepared by dissolving known amounts of preasphaltenes, asphaltenes and oils obtained by soxhlet separation of whole liquid product from preparatory liquefaction experiments (6). Peak height measurement and response factors were used to calculate the percentages of preasphaltenes, asphaltenes and oils for the THF soluble product. All yield and conversion data were calculated on a dry mineral matter-free (dmmf) coal basis, which included a correction for the conversion of pyrite content of the coal to pyrrhotite.

RESULTS AND DISCUSSION

Process Course and Selectivity

Two ternary diagrams of product/by-product distributions for the coal liquefaction experiments previously described are shown in Figures 1 and 2. Conversion data for the various experiments are represented by the following symbols-- ● Co/Mo catalyzed; ■ Mo-naphthenate catalyzed; and □ naphthenic acid blank. In Figure 1, asphaltene conversion is plotted against oil conversion (both wt % dmmf basis) and in Figure 2, the sum of mole percent oil and asphaltene conversion is plotted vs mole percent hydrocarbon gas conversion. Because of the large difference between molecular weight of gases (CH_4 to C_4H_{10} -- 16-58) and other products (e.g., oils--200 to 400), the mole percent basis is used to more precisely represent the ternary diagrams involving hydrocarbon gases. For the purpose of calculating mole percentages, average molecular weights of 2400, 1200, 600 and 300 were assumed for the fractions of IOM, preasphaltenes, asphaltenes and oils. These values approximately correspond to the middle of the molecular weight distribution ranges for these fractions (7). Moles of gases produced were experimentally determined as previously described.

Figures 1 and 2 illustrate several general observations which can be made about the coal liquefaction process. First, although the liquefaction process is complex, involving myriad chemical species, its course can be quantitatively described by simple diagrams relating groups of compounds which react in similar and predictable manners.

These diagrams may roughly be considered the kinetic analog of equilibrium phase diagrams in which the number of components of a system is the smallest number of independently variable constituents. The composition of the liquefaction reaction mixture is given by the fractions explicitly represented by the x and y axes, and a remainder portion represented by the length of a horizontal tie line from a point on the curve to the diagonal axis connecting the x and y axes. For Figure 1, asphaltene and oil conversion are given by the y and x axis and preasphaltene, IOM and gases by the tie line. Second, the hyperbolic relationships for the conversion of the fractions shown in the figures represent unique reaction paths for the Co/Mo catalyzed reactions, over a wide range of operating conditions--time, temperature and reactor type. Deviations from this hyperbola represent conditions which change the process course, for example, the onset of competing pyrolysis reactions at high temperatures which form coke and gas. This indicates that the selectivity for a coal liquefaction catalyst, with respect to product groups, may be uniquely described by hyperbolic relationships. Support for this hypothesis is given by the analysis of the selectivity for a set of two unidirectional, consecutive reactions for which the selectivity may be described by relative concentrations given by hyperbolic equations of one constant (2, 8).

The utility of ternary diagrams and hyperbolic relationships exemplified by Figures 1 and 2 is that they may be used to rapidly screen for catalyst selectivity. Once hyperbolic relations are derived for a baseline catalyst, the selectivity of another catalyst may be screened by comparison of its product/by-product distributions for one or two experiments with the hyperbola of the baseline catalyst. It can be seen in Figure 1 that the point for the Mo naphthenate experiment falls below the curve for Co/Mo but above the blank experiment. This indicates that the order of asphaltene to oil selectivity is:

$$\text{Blank} < \text{Mo-naphthenate} < \text{Co/Mo}.$$

In Figure 2, the sum of the coal conversion products, oils and asphaltenes, are plotted as a function of unwanted by-product hydrocarbon gas conversion. Again, the Mo-naphthenate point falls between the Co/Mo curve and the blank. Thus Mo-naphthenate, at the concentration used is not as selective for asphaltene and oil conversion as Co/Mo, but does promote a better product/by-product ratio than the non-catalyzed experiment.

Hydrogen Consumption Diagram

Another useful relationship developed to determine the efficiency or selectivity of a hydrogenation catalyst with respect to process hydrogen consumption is illustrated in Figure 3, a plot of the sum of oil and asphaltene conversion (wt %, dmmf) as a function of the fraction of hydrogen consumed by production of hydrocarbon gases (the ratio of the weight of hydrogen in the hydrocarbon gases to the hydrogen consumed). Again, a wide range of experimental conditions for hydrogenation of coal catalyzed by Co/Mo can be represented by a single curve. This diagram provides a more significant selectivity test than the hyperbolic correlations in that it relates directly to a primary goal of catalyst development for direct coal liquefaction--maximizing the yield of distillate products with respect to hydrogen consumption. Figure 3 illustrates that hydrogenation efficiency of Co/Mo-catalyzed conversion of coal to oil and asphaltenes sharply

decreases above conversions of about 80%. Points representing experiments for other catalysts falling below the Co/Mo curve indicate that these catalysts are less efficient than Co/Mo with respect to hydrogen consumption. The point representing the Mo-naphthenate experiment falls close to the Co/Mo curve indicating an efficiency nearly equal to Co/Mo, while the blank experiment (naphthenic acid) shows that non-catalyzed coal conversion is much less efficient in hydrogen consumption.

REFERENCES

1. F. Breimer, H. I. Waterman and A. B. R. Weber, J. Inst. Petroleum, 43, 297 (1957).

2. H. I. Waterman, C. Bodhouwer and D. Th. A. Huibers, "Process Characterization", Elsevier, New York, 1960.

3. L. C. Doelp, W. Brenner, and A. H. Weiss, I&EC Proc. Des. Dev. 4, 92 (1965).

4. M. G. Thomas and D. G. Sample, "Catalyst Characterization in Coal Liquefaction", SAND-80-0123, Sandia National Laboratories, June 1980.

5. B. Granoff, et al., "Chemical Studies on the Synthoil Process: Mineral Matter Effects," SAND-78-1113, Sandia National Laboratories, June 1978.

6. A. W. Lynch, Sandia National Laboratories, personal communication, 1981.

7. D. D. Whitehurst, M. Farcasiu and T. O. Mitchell, "The Nature and Origin of Asphaltenes in Processed Coals," EPRI AF-252, February 1976.

8. A. H. Weiss, "Considerations in the Study of Reaction Sets," Catalysis Reviews 5, 1972.

Key to Figures

Number	Symbol	Reactor	Catalyst	T(°C)	t(min)
1	●	Micro	Co/Mo	350	15
2	●	"	"	375	15
3	●	"	"	425	0.5
4	●	"	"	400	15
5	●	"	"	425	10
6	●	"	"	425	15
7	●	"	"	425	40
8	●	"	"	425	80
9	●	Autoclave	"	425	30
10	●	"	"	425	120
11	■	Micro	Mo-Naphth	425	30
12	□	"	Blank	425	30

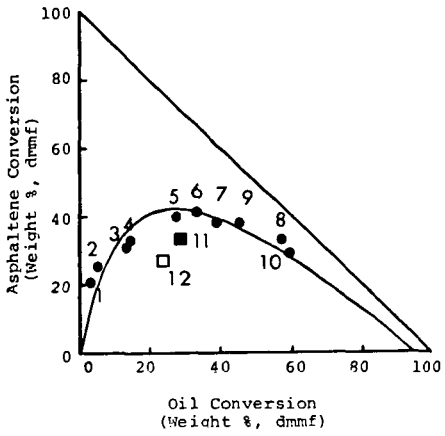

Figure 1. Ternary diagram of asphaltene vs. oil conversion. The curve, given by the equation

$$y = \frac{x(95-x)}{16.9+1.00x}$$

represents the process course for the Co/Mo catalyzed experiments.

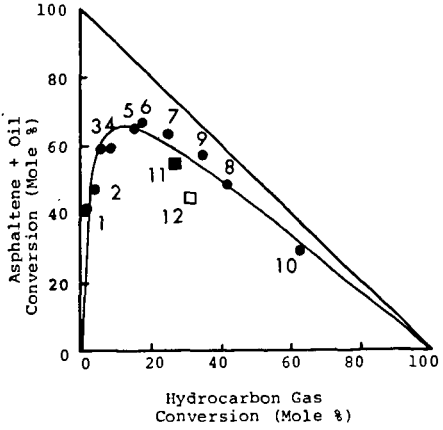

Figure 2. Ternary diagram of the sum of asphaltene and oil conversion vs. hydrocarbon gas conversion. The curve is given by the equation

$$y = \frac{x(100-x)}{2.35+1.15x}$$

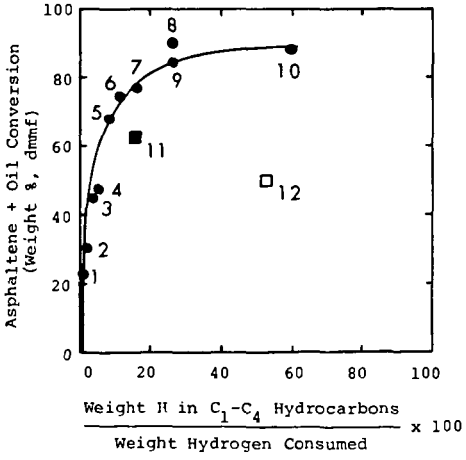

Figure 3. Hydrogen consumption diagram for direct coal liquefaction experiments. Curve represents Co/Mo catalyzed experiments.

The Effect of Pressure and Gas Composition on the Fluidity of Pittsburgh No. 8 Coal

M. S. Lancet
F. A. Sim

Conoco Coal Development Company
Research Division
Library, PA 15129

INTRODUCTION

The Gieseler method[1] of measuring the fluidity of coal has long been a parameter used by the steel industry for the evaluation of coke oven feedstocks. This analytical technique in which the rotational speed of a rabble arm stirrer held in a packed sample of ground coal is measured as it is twisted with a known torque while the sample is heated through the plastic range, is a measure of the pseudo viscosity of the molten or semi-molten coal.

The interest in recent years in the gasification of Eastern U.S. bituminous coals has led to concern over potential coking and handling problems of these coals as they are fed to the gasifier. Conoco's experience with the gasification of two highly fluid Eastern coals during the DOE sponsored Technical Support Program for the British Gas/Lurgi slagging gasifier project suggested that these coals demonstrate significantly different coking and fluidity properties under gasifier conditions than they do at standard atmospheric conditions. Hence Conoco began a program for the evaluation of gasifier feedstocks which includes examining the coking properties at simulated gasifier conditions.

As a part of this overall program Conoco has designed and built a pressurized Gieseler Plastometer in which it is possible to measure the fluidity of coals in atmospheres of any desired composition and at total pressures up to 450 psig. The initial series of tests in this apparatus, reported here, is a study of the effect of nitrogen and hydrogen pressure on the fluidity of a Pittsburgh No. 8 seam coal. Nitrogen was chosen as an "inert" gas to examine only the effect of total pressure while hydrogen - probably the most reactive gas in a gasifier - was chosen as a first approximation to a gasifier gas.

EXPERIMENTAL

Apparatus

The basic apparatus consists of a Standard Instrumentation Model P-11R research version Gieseler Plastometer with the measuring head and solder pot mounted in a pressure vessel and the associated electronics located externally. Figure 1 is a design drawing of the apparatus. The pressure vessel is fabricated from a 30" long, 10" dia schedule 40 pipe, capped at the bottom and flanged at the top. A solder pot rests on a perforated steel plate at the bottom and the measuring head and crucible assembly are suspended from the top flange. A sight gauge is provided to insure proper alignment during the lowering of the crucible into the solder pot.

Electrical leads are passed into the pressure shell through conax pressure seal fittings. The vessel is pressurized through a half inch inlet port and the pressure is monitored during a run via a 0-600 psig pressure indicator. The vessel has a pressure relief valve set at approximately 550 psig to insure against accidental over pressurization. Figure 2 is a flow diagram for the pressurized Gieseler plastometer at Conoco Coal Development Company.

Procedure

The coal is sampled, ground and packed into the crucible in the standard manner.[1] The packed crucible assembly is then connected to the measuring head and the whole assembly is lowered, along with the attached top flange, into the pressure vessel. When the flange is flush with the top the crucible is at the proper position in the solder bath which is preheated to 320°C. After lowering, the flange is sealed and the vessel evacuated. The vessel is pressurized with the desired gas and, as soon as the solder pot temperature recovers to 320°C, the run is begun.

The sample is heated at a constant rate, normally 3°C/min, and the rotation of the rabble arm stirrer is constantly monitored and is printed out each minute. The unit of dial divisions per minute (DDPM) which is actually 100 times the rotational speed in RPM are the standard Gieseler fluidity units.

As the coal sample is heated it begins to soften and the stirrer begins to rotate. The point at which this occurs is called the softening temperature, T_S. Further heating the sample leads to an increase of the stirrer rotation until the maximum rate is reached at the temperature of maximum fluidity, T_M. Finally as the temperature of the coal is raised past T_M the fluidity begins to decrease until the temperature of resolidification, T_R, is reached. At this point all stirrer rotation stops and the sample is normally fully coked.

At the end of a run the vessel is depressurized and the sample, crucible and head assembly are removed for cleaning. A complete run requires about 1.5-2 hours.

Results and Discussion

The coal used in this work was from Montour No. 4 mine and is a high volatile, highly caking Eastern U.S. bituminous coal from the Pittsburgh No. 8 seam. The run of mine (ROM) coal was screened at 3/4" and only the washed +3/4" lumps were used in this work. The coal was stored in a sealed plastic bag and was ground for the Gieseler work just prior to use. Table 1 shows the proximate and ultimate analyses of this coal together with the energy content, the standard Gieseler fluidity and Free Swelling Index (FSI).

A total of 44 runs were made in this study, 23 with prepurified nitrogen and 21 with hydrogen. The results of these experiments are given in Table 2. The fluidity given at each point is the average of the maximum fluidity value from at least two runs and for the unpressurized cases, four runs. The agreement between duplicate runs was always better than ± 10%.

Since the maximum fluidity obtainable at standard Gieseler conditions of 1.40 oz·in (141 gm·cm) of torque is about 28,000 most of the data obtained here were at lower torque settings of either 0.45 oz·in (45 g·cm) or 0.30 oz·in (30 g·cm). All the data reported in terms of the standard torque value. This value was obtained by multiplying the measured fluidity by the ratio of standard torque to the torque value actually used (i.e., 3.11 or 4.67 for the two cases in this work). When duplicate runs were made using the different torque settings the agreement between the corrected fluidities was as good as that obtained for duplicate runs at the same torque setting. This suggests that, at least in the case of highly fluid coals, a coal in its plastic state may resemble a Newtonian liquid.

If it is possible to treat this coal as a Newtonian liquid we can, by calibration of our plastometer crucible and stirrer with viscosity standards, estimate the viscosity of the coal in its plastic state. Such calibration gives

the following relationship between "pseudo" viscosity, η (poise) and fluidity, F (DDPM).

$$\log_{10}\eta = - \log_{10}F + 7.257 \qquad 1)$$

This suggests that the apparent viscosity of the Montour No. 4 coal used in this work, at the temperature of its maximum fluidity, lies between about 170 and 2000 poise.

Figure 3, a plot of the data in Table 2 clearly shows the effect that pressure has on the maximum fluidity of this particular coal. Initially, the fluidity is increased quite rapidly by raising the pressure of both hydrogen and nitrogen, however, while the effect is seen to continue almost linearly for the hydrogen pressure, the nitrogen pressure has only a limited effect above about 100 psig. These efforts are consistent with those observed by Kaiho and Toda[2] who made a similar study for the medium fluidity, weakly caking Akabira coal. The initial large increase in maximum fluidity with pressure is probably due to the retarded rate of volatile evolution. With the more volatile and hence presumably less viscous components held in the "plastic" coal longer, an increase in maximum fluidity is logical.

Another, although seemingly less likely, possibility for the increased fluidity is the increased dissolution of the gas used and/or coal gases in the coal liquids which may lead to a decrease in the viscosity of the coal system and hence to an increase in the fluidity. The higher fluidities observed with nitrogen vs. hydrogen in the range 0-150 psig may be an experimental artifact caused by slightly lower heating rates for the hydrogen cases due to the higher thermal conductivity of hydrogen. It is known that heating rate is directly related to the fluidity of certain coals.[3]

As the pressure of the inert gas, nitrogen, is further increased, the leveling off of the fluidity may be due to approaching the limits of the effect of pressure alone on fluidity. Possibly pressures of 100-150 psig are sufficient to retard the escape of volatiles until the plastic coal has reached its temperature of maximum fluidity. Above these pressures it appears that any additional volatiles which are trapped have little effect on the fluidity.

The much more dramatic effect of hydrogen pressure on the maximum fluidity, Figure 3, is probably due to reactions between the hydrogen and components in the coal as well as the retardation of volatile escape. This observed hydrogen effect is, of course, consistent with the liquefaction of coal by very high pressures ($\gtrsim$ 2000 psig) of hydrogen at approximately the temperature of maximum fluidity.

While the pressure has a major effect on the maximum fluidity of the coal it shows almost no relation to the temperature of maximum fluidity. Also no effect of pressure on the softening point or the resolidification temperature was observed. Throughout this work the softening temperature was 360 ± 5°C, the solidification temperature was 475 ± 5°C and the temperature of maximum fluidity was 435 ± 5°C.

REFERENCES

1. Standard Method of Test for Plastic Properties of Coal by the Constant-Torque Gieseler Plastometer. ASTM Designation: D 2639-71.
2. Kaiho, M. and Toda, Y., Change in the Thermoplastic Properties of Coal Under Pressure of Various Gases. FUEL 58, 397 (May, 1979).
3. Van Krevelen, D. W., Huntjens, F. J., and Dormans, H. N. M., "Chemical Structures and Properties of Coal IVI--Plastic Behavior on Heating," Fuel 35, 462 (1955).

TABLE 1

Analysis of Montour No. 4 Coal

Proximate Analysis		
Moisture	(%)	1.69
Ash	(%)	6.97
Volatile Matter	(%)	38.79
Ultimate Analysis (Dry Basis)		
C	(%)	76.81
H	(%)	5.16
N	(%)	1.73
S	(%)	1.35
O (By Diff.)	(%)	7.98
Ultimate Analysis (MAF)		
C	(%)	82.67
H	(%)	5.55
N	(%)	1.86
S	(%)	1.46
O (By Diff.)	(%)	8.46
Energy Content (Dry Basis)		
HHV (Btu/lb)		14,110
Free Swelling Index		7-1/2
Fluidity (DDPM)		9300

TABLE 2

Fluidity of Montour No. 4 Coal in Nitrogen and Hydrogen Atmospheres

Gas	Pressure (psig)	Fluidity(1)
Nitrogen	0	9,300
	50	22,300
	100	38,800
	150	44,600
	200	46,800
	250	48,100
	300	49,100
	350	51,200
	400	51,900
Hydrogen	0	9,400
	50	19,400
	100	34,700
	150	40,000
	200	51,100
	250	65,900
	300	80,800
	350	95,100
	400	104,900

(1) Fluidity rounded to nearest 100 DDPM based on average of at least 2 measurements.

All runs at 3 ± .1°C/min heating rate.

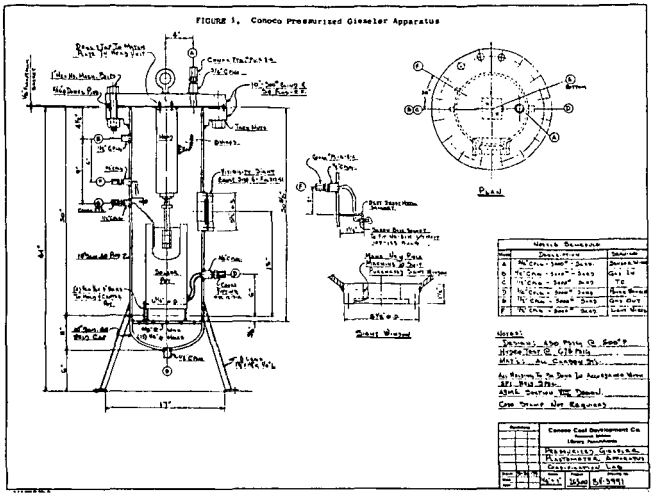

FIGURE 2

PRESSURIZED GIESELER PLASTOMETER FLOW DIAGRAM

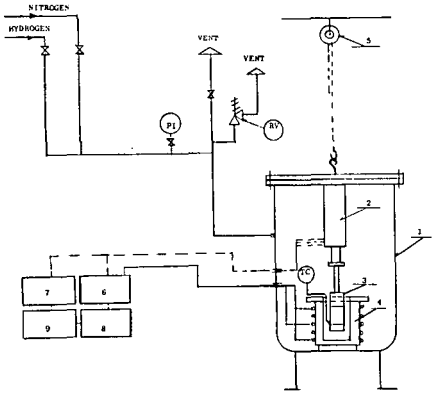

Legend

1 PRESSURE VESSEL
2 PLASTOMETER HEAD
3 RETORT
4 FURNACE
5 HOIST
6 FURNACE CONTROLS
7 PLASTOMETER CONTROLS
8 PRINTER
9 PLOTTER

FIGURE 3

THE EFFECT OF PRESSURE ON THE FLUIDITY OF MONTOUR NO. 4 BITUMINOUS COAL

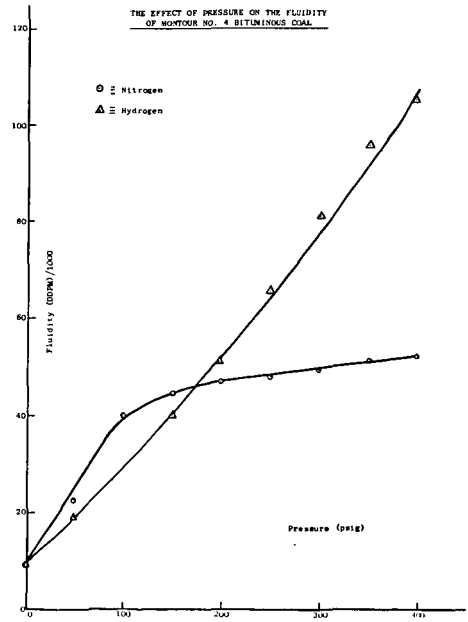

DIFFUSION OF IONS INTO COAL: METHOD OF MEASUREMENT, ORDER OF MAGNITUDE AND DIRECTIONAL EFFECTS

By: Attar, A. and Warren, D.
Dept. Chem. Eng., N.C.S.U., Raleigh, N.C. 27650

1. INTRODUCTION

Incorporation of metal ions from solution into the coal structure is becoming a useful method to achieve high contact between the coal surface and the metal ions. However, no data were found in the literature relative to the diffusivity of ions in coal. In this work, preliminary results are reported on the rate of diffusion of ions into coal and on the rate of leaching of ions from coal.

The main results found are that: 1) the diffusivity of ions varies in different directions of a vitrinite particle, relative to the direction of the bedding, and 2) the diffusion coefficient of calcium ions is of the order of 10^{-12} cm^2/sec in the direction of the bedding and 10^{-13} cm^2/sec in the direction perpendicular to the bedding.

2. EXPERIMENTAL

The coal particles to be examined were hot pressed (70°C, 15000 psi) in polymethyl metacrylate stubs, 3/4" in diameter and 3/8 - 1/2" thick. The stubs were cut through the coal particles and the exposed surfaces were polished under petroleum ether, using cloths 220, 400 and 600 successively. Finishing was done using 0.3 micron alumina powder in petroleum ether. The polished surface was sputtered with carbon and grounded with silver paint.

The surfaces were scanned using a 20000 Volt electron beam and the K_α x-rays from the calcium were collected within $\pm$ 2 eV. The resolution between the Ca (K_α) lines and the K (K_β) lines appears to be adequate to allow separation of the calcium.

Scanning of the coal surface was done at the rate of 3 microns/minute and plotted at either 3 microns/inch or 16 microns/inch. The total counts of x-rays were integrated and printed every 20 seconds.

3. MODES OF CALCIUM PENETRATION

The results that are obtained are a signal proportional to the number of atoms of calcium in a segment of volume of the coal specimen, with a shape of a droplet of tear, with an average length of about 6-10 microns and a diameter of 3-5 microns near the surface. This volume will be heretofore titled the "probe volume." Obviously, the signal obtained will not resolve differences in concentrations of calcium associated with features smaller than the probe volume and consequently the signal is only an average measure of the calcium present in the probe volume in all forms. A special mathematical method is being developed to "deconvolute" the signal in order to resolve finer features.

The main modes by which calcium could have penetrated into the coal are:

1. Penetration of Ca^{+2} through pores.
2. Diffusion of Ca^{+2} ions into the solid matrix and forming a Ca-containing intercolate.

Figure 1 shows the form of the signal expected when penetration of Ca occurs into the solid, through a pore oriented parallel to the direction of travel of the beam and through a pore presented perpendicular to the direction of travel of the beam. Since the diffusion coefficient in liquid is substantially larger than in solid, a relatively low incorporation occurs via the micropores ($r < 0.01$ M) and most of the calcium incorporation occurs via the mesopores and the macropores.

Several models can be used to interpret the experimental results. First, the models and their solutions will be described and then data will be presented and interpreted.

3.1 Effective Diffusion through a Thin Layer of Solid

In the case of a thin layer the unidirectional model is applicable. Thus:

$$\frac{\partial c}{\partial t} = D_s \frac{\partial^2 c}{\partial x^2} , \tag{1}$$

$$c(0,x) = 0 , \tag{2}$$

$$c(t,0) = c_0 , \tag{3}$$

and

$$c(t,\infty) = 0 . \tag{4}$$

The solution is:

$$\frac{c}{c_0} = \text{erfc}\left(\frac{x}{2\sqrt{D_s t}}\right) . \tag{5}$$

x is the distance from the surface, D_s is the effective diffusivity coefficient, and t is the penetration time. The concentration at (x,t) is c and c_0 is the concentration near the surface. The error function complementary, erfc, is defined by:

$$\text{erfc}(z) = 1 - \frac{2}{\sqrt{\pi}} \int_0^z e^{-2}du . \tag{6}$$

Obviously:

$$\int_0^\infty e^{-u^2} du = \frac{\sqrt{\pi}}{2} \tag{7}$$

was used to normalize the distributions.

Equation (5) is useful to interpret data for diffusion through a thin layer of solid or effective diffusivity through heterogeneous features smaller than the depth of penetration.

3.2 Effective Diffusion Through a Pore Full with Liquid

$$\frac{\partial c}{\partial t} = D_L \frac{\partial^2 c}{\partial x^2} , \tag{8}$$

$$c(0,t) = c_0 , \tag{9}$$

$$c(x,0) = 0 , \tag{10}$$

$$\frac{\partial c}{\partial x}(\ell,t) = 0. \tag{11}$$

The solution is:

$$\frac{c}{c_0} = 1 - \sum_{n=1}^{\infty} \frac{4e^{-\lambda_n^2 D_L t}}{(2n-1)\pi + (-1)^{n+1}} \sin \lambda_n x \tag{12}$$

$$\lambda_n = \frac{(2n-1)\pi}{2\ell} . \tag{13}$$

The total material diffused after time t is:

$$M = -\int_0^t D\left(\frac{\partial c}{\partial x}\right)_{x=0} A dt = + 4DAc_0 \int_0^t \sum_{n=1}^{\infty} \frac{e^{-\lambda_n^2 D_L t} \lambda_n}{(2n-1)\pi + (-1)^{n+1}} dt$$

$$= - 4DAc_0 \sum_{n=1}^{\infty} \frac{1 - e^{-\lambda_n^2 D_L t}}{[(2n-1)\pi + (-1)^{n+1}] \lambda_n D_L} . \tag{14}$$

The use of equation (14) is not immediately obvious since the total area of pore mouth/unit mass, A, is not readily available and because λ_n depends on the distribution of pore lengths.

4. TESTS PERFORMED

The experimental tests performed can be divided into two classes:

A. Tests used to develop the method.
B. Tests on samples exposed to calcium acetate solution at room temperature and atmospheric pressures.

4.1 Method Development

The method that has been developed was described in the previous section. The possibility of inaccurate results due to overlap of consequative scanning intervals should be addressed. Since the beam is about 4 microns in diameter and a printout is generated every twenty seconds, each printout represents counts taken over 4 microns diameter beam which moved 1 micron. Thus, the second printout will include counts taken from some of the calcium atoms which contributed to the first counts. In addition, since the electron beam damages the surface to some extent, the results may be distorted. The data show, however, that in three Ca curves almost on the same coal surface path, forward, backward and forward again, very little distortion occurred over about 200 microns.

4.2 Incorporation Tests

Samples of vitrinite from an Illinois #6 (Monterey Mine) and of the Colberg seam (W. Va.) were:

1. Leached with HCl 2:1 per 20 min.
2. Mixed with 0.05M calcium acetate solution at room temperature for 78 hours, dried and stored under nitrogen until fixed in the polymer.

The results on the HCl treated samples had a large statistical error built into them but show that:

1. Leaching of calcium occurs through a boundary layer.
2. The thickness of the leached layer is different in different directions of the seam.

For each leaching, the governing equation is:

$$\frac{c}{c_0} = \text{erf}\left(\frac{x}{2\sqrt{D_e t}}\right) . \qquad (15)$$

The data collected for the first fourteen microns near the surface and the background information are tabulated in Table 1. In accord with equation (15), a plot of $x/(2\sqrt{D_e t})$ vs. x should give a straight line, with slope of $1/(2\sqrt{D_e t})$. The line will not necessarily intersect with the origin, since there is uncertainty relative to the exact location of the surface of the particle. Figure 2 shows that the slope of the line is 806.4 cm^{-1} which corresponds to $D_e = 1.68 \cdot 10^{-12}$ cm^2/sec since the leaching time was 78 hours. Similar calculations for scans in different directions yielded values of D_e in the range of 10^{-9} - 10^{-13} cm^2/sec. However, it appears that 10^{-12} cm^2/sec can be considered a representative number for this coal.

Many samples of coal were treated for periods of 1 hour to 5 days with excess solution of 0.05M calcium acetate in water. The samples were fixed in polymethyl metacrylate base, sputtered with carbon and analyzed as before. The data seem to indicate two modes of penetration of calcium: (A) by diffusion through the surface, and (b) by filling up of pores. Schematically, the calcium signal shows three types of behavior as the electron beam travels from the outside of the particle in (A) gradual decrease in calcium concontration in accord with the diffusion through the surface, i.e., erfc $[x/(2\sqrt{Dt})]$; (B) large and reasonably fixed level of signal, corresponding to scanning along a pore; and (C) a Gaussian-shaped peak, corresponding to traveling across a pore.

Table 1. HCl leached coal

Distance from Coal Surface (microns)	Counts	c/c_0 $c_0 = 110$	$\text{erf}^{-1}(\frac{c}{c_0}) = \frac{x}{2\sqrt{D_e t}}$
-4	2	0.018	-
-3	1	0.009	-
-2	1	0.009	-
-1	3	0.027	-
0	3	0.027	-
+1	10	0.091	0.091
2	12	0.019	0.098
3	13	0.118	0.105
4	20	0.182	0.163
5	36	0.327	0.298
6	47	0.427	0.398
7	52	0.473	0.447
8	69	0.627	0.630
9	74	0.673	0.695
10	71	0.645	0.654
11	77	0.700	0.738
12	86	0.782	0.873
13	73	0.664	0.863
14	96	0.873	1.085

The results of scans of a sample of coal from the Colberg seam, West Virginia, in two orthogonal directions are described below. The data for the first 21 microns are given in Tables 2 and 3. Figure shows that the penetration in the vertical direction is much slower but more uniform than penetration in the horizontal direction. The effective diffusivity coefficient in the vertical direction is about two orders of magnitude smaller than in the horizontal direction.

Table 2. Scanning of Colberg seam coal in the direction of the grain

Distance from Surface (microns)		Counts	$\frac{c}{c_0}(c_0=1973)$	$\text{erfc}^{-1}(\frac{c}{c_0})$
	-2	1005	0.5094	-
Coal	-1	1019	0.5165	-
Particle →	0	1973	1.0000	-
Surface	1	1860	0.9427	0.051
	2	1755	0.8899	0.099
	3	1520	0.7704	0.208
	4	1336	0.6771	0.294
	5	1139	0.5773	0.398
	6	941	0.4769	0.504
	7	818	0.4146	0.574
	8	725	0.3675	0.638
	9	566	0.2869	0.755
	10	591	0.2995	0.730
	11	461	0.2336	0.841
	12	442	0.2240	0.860
	13	444	0.2250	0.858
	14	424	0.2149	0.877

Table 3. Scanning of Colberg seam coal perpendicular to the direction of the grain

Distance from Surface (microns)	Counts	$\frac{c}{c_0}$ (c_0=1973)	$erfc^{-1}(\frac{c}{c_0})$
-21	60	0.1881	-
-20	61	0.1912	-
-19	74	0.2319	
-18	61	0.1912	
-17	71	0.2226	
-16	80	0.2508	
-15	93	0.2915	
-14	80	0.2508	
-13	106	0.3323	
-12	141	0.4420	
-11	166	0.9204	
-10	166	0.5204	
- 9	184	0.5768	
- 8	217	0.6802	
- 7	205	0.6426	
- 6	253	0.7931	
- 5	278	0.8715	
- 4	271	0.8495	
- 3	282	0.8840	
- 2	260	0.8150	
- 1	278	0.8715	
0	319	1.0000	0.0000
1	264	0.8276	0.1580
2	281	0.7555	0.2210
3	301	0.9436	0.0510
4	262	0.8213	0.1590
5	238	0.7461	0.2280
6	234	0.7335	0.2480
7	235	0.7367	0.2481
8	223	0.6990	0.2750
9	209	0.6552	0.3150
10	239	0.7492	0.2280
11	232	0.7272	0.2460
12	209	0.6552	0.3150
13	175	0.5486	0.4310
14	221	0.6928	0.2790
15	202	0.6332	0.3380
16	224	0.7072	0.2750

5. CONCLUSIONS

The main objectives of this study were achieved:

1. A method has been developed which allows examination of the penetration of calcium ions into coal.
2. The method was applied to study the penetration of calcium into coals.

The data show that calcium penetrates into coal in two main modes: via pores and via regular diffusion. The diffusivity coefficient in the horizontal direction relative to the seam is 10^2 - 10^3 times larger than in the vertical direction. In the horizontal direction it is 10^{-8} - 10^{-11} cm^2/sec while in the vertical direction it is of the order of 10^{-12} - 10^{-13} cm^2/sec. $D_{bedding} = 7.6 \cdot 10^{-11}$ cm^2/sec. $D_{vertical} = 9.7 \cdot 10^{-13}$ cm^2/sec.

Figure 1

EFFECT OF DIFFERENT FEATURES
ON THE PROBE SIGNAL

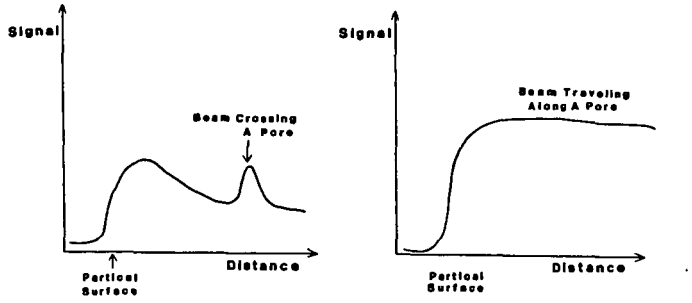

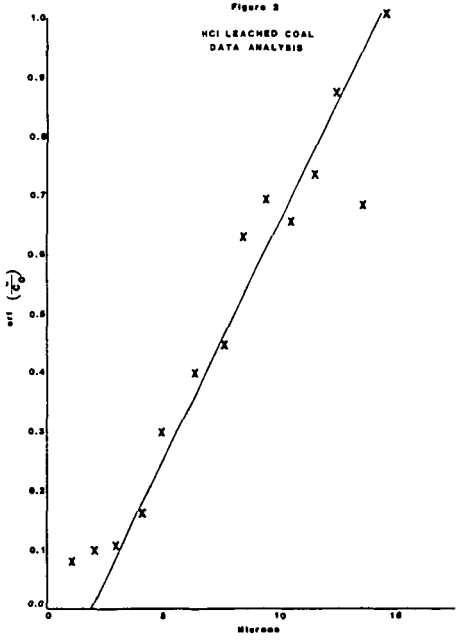

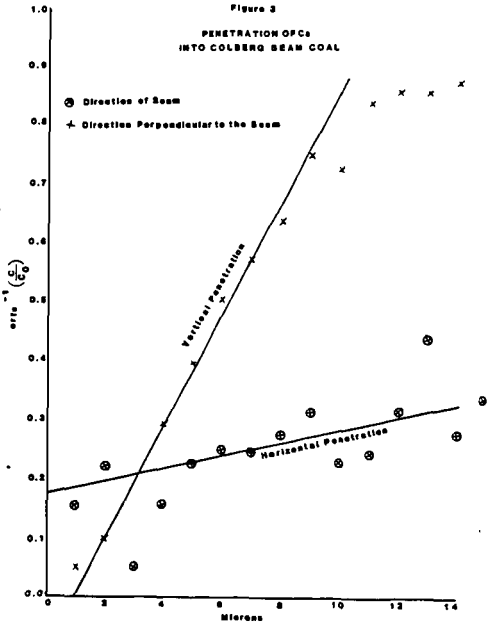

Effect of Composition on Freezing Points of Model Hydrocarbon Fuels

W. A. Affens, J. M. Hall, S. Holt, R. N. Hazlett

Naval Research Laboratory, Washington, D. C. 20375

INTRODUCTION

Freezing Points of Jet Fuels

Jet aircraft are frequently exposed to low operating temperatures and it is essential that their fuels not freeze in these environments. Plugging of filters, pumpability, and related fuel system operational problems are dependent on freezing point, and for this reason, jet fuel specifications include requirements for maximum freezing point. Commercial jet fuel (Jet A, Aviation Turbine Fuel, ASTM D 1655-80), for example, is required not to freeze above -40°C. Military jet fuels, because of world wide operations, have even lower temperature requirements. The maximum acceptable freezing points for Air Force fuels (JP-4 and JP-8 Aviation Turbine Fuels, MIL-T-5624L and MIL-T-83133A respectively) are -58° and -50°C; and the Navy's JP-5, (MIL-T-5624L, High Flash Point Aviation Turbine Fuel) has a maximum of -46°C.

The low temperature properties of a jet fuel (freezing point, pour point, viscosity), as well as some of its other properties, are controlled by the nature and concentrations of its components (chemical composition). Unfortunately, many components of a fuel which tend to lower freezing point (smaller hydrocarbons of higher vapor pressure), will also lower the flash point. In the case of JP-5, because of its relatively high minimum requirement for flash point (60°C) for reasons of ship safety, and its low maximum requirement for freezing point (-46°C), it is not always practical to produce JP-5 from all available crudes. These restraints limit the amount of JP-5 which can be produced from a barrel of crude oil and the problem exists for both conventional JP-5 (from petroleum) and for JP-5 from syncrudes.

Freezing Point and Composition

It has been known that molecular size and symmetry play an important part in the phenomenon of crystallization from solution and that this also applies to solutions of hydrocarbons. Dimitroff et al (1,2), studying the effect of composition on several types of fuels, found that the saturate fraction exerted the greatest influence on raising the freezing point and that the presence and amount of high-temperature freezing hydrocarbons had a major influence. They reported that in some cases the aromatic fraction was important and that in general all hydrocarbons play a part in fuel crystallization. Petrovic and Vitorovic (3) found a correlation between the sum of the concentrations of the three largest straight chain alkanes and freezing point in the jet fuels which they studied. Antoine reported on studies of 32 samples of jet

fuel derived from oil shale and coal syncrudes (4) and concluded that the concentrations of the long straight chain molecules in the fuels exert influence on the freezing point but are not the complete controlling factor. Solash et al (5) at this laboratory investigated jet fuels derived from various sources and reported that the freezing points were related to the amount of the largest n-alkane present (but not the total n-alkane concentration) in these fuels. These findings were not in agreement with the correlation of Petrovic and Vitorovic. Solash et al plotted log (mol% C_{16}) vs. the reciprocal freezing point of 11 fuels and found reasonable adherence to a solubility plot. They concluded that the freezing point of a fuel is not a simple function of fuel composition and that much more work must be done before a coherent theory of freezing point can be developed for multi-component mixtures.

It was decided to extend our freezing point studies to model hydrocarbon fuel mixtures, with emphasis on the higher n-alkanes, in order to learn more concerning the effect of composition on freezing point.

EXPERIMENTAL

Defining Freezing Point

"Freezing Point," as applied to jet fuels and related mixtures, is defined by the ASTM (6) as "..that temperature at which crystals of hydrocarbons formed on cooling disappear when the temperature of the fuel is allowed to rise". This, of course, is really a "melting point," since "freezing point" is the temperature at which crystals start to crystallize out. However, the two phenomena take place at almost equivalent temperatures, and the term "freezing point" will be used here because of its wide use in the fuel literature.

Determination of Freezing Point

Freezing points were determined by the ASTM method D2386 for aviation fuels (7) with some modifications. Temperature readings were made by means of a thermocouple (Type "J") - potentiometer-recorder system, and liquid nitrogen was used as the refrigerant. Stirring was done mechanically.

Hydrocarbons

The hydrocarbons used were 99% pure grade. The decalin (decahydronaphthalene) was found to consist of 62.7% (w/w) of the trans isomer and 37.3% cis isomer by gas chromatography. The "Isopar-M" kerosene consisted of a relatively high boiling, low freezing, narrow-cut isoparaffinic solvent whose average molecular weight was 191 (8).

RESULTS AND DISCUSSION

n-Alkanes in Isopar-M

Solutions of six n-alkanes (C_{12} - C_{17}) in Isopar-M at various concentrations (mol %) were prepared and their freezing points (T_m) determined. Reciprocal freezing points ($1/T_m$) vs log of concentrations are plotted in Figure 1 for each alkane. The temperature scale (ordinate) of the graph is reversed in order to show temperature increase going up the graph. It is seen in the figure that the data points fit the straight lines fairly well so that there is good adherence to a typical solubility plot (ideal freezing point curve). The lines shown in the graph were derived by means of a linear regression treatment of the data and are a best fit of the data. From their slopes and intercepts, heats (ΔH_m) and entropies (ΔS_m) of fusion and extrapolated freezing points ($T_{m,o}$) of the pure alkanes were calculated by means of the Van't Hoff ideal solubility equation (9-12), and the thermodynamic relationship between ΔS_m, ΔH_m and $T_{m,o}$ (13).

$$\text{Ln } X = - \Delta H_m/RT_m + \Delta H_m/RT_{m,o} \qquad 1)$$

$$\Delta S_m = \Delta H_m/T_{m,o} \qquad 2)$$

where R is the gas constant, and X represents molar concentration. This approximate equation, which describes the variation of freezing point with concentration, is based on several simplifying assumptions including that ΔH_m is independent of temperature, and that Raoult's law is obeyed. Derived freezing point data from the Isopar-M solutions are shown in Table I with literature values of pure n-alkanes (13, 14) shown for comparison.

It is seen in the table that the experimentally derived and literature $T_{m,o}$ values are in good agreement, but this is not always the case for ΔH_m and ΔS_m. For ΔH_m and ΔS_m, the agreement is good only for the even carbon numbered alkanes, but there is poor agreement for the odd numbered compounds. It has long been known (9) that freezing and melting point data of pure compounds in some homologous series often exhibit the phenomenon of "alternation". In these series, such as the n-alkanes, with each additional CH_2 group, alternately small and large increases in a given property are observed (9). This can be seen for each of the three properties in Table I for both the literature data for the pure alkanes, and the values derived from the Isopar-M solution freezing points. It has been shown (9) for the higher members of a homologous series, that ΔH_m and ΔS_m values fall on two linear curves when plotted against carbon number. In this work, the odd and the even carbon numbered alkane data also form two separate straight lines respectively when ΔH_m or ΔS_m are plotted against carbon number. There was, however, a much wider variation between the odd and even data points for the literature values than between that of the experimentally derived points in this study.

Solvent Effect

In a second set of freezing point experiments, the effect of solvent was investigated. Solutions were prepared for n-tetradecane, n-hexadecane, and naphthalene in different solvents and at several concentrations. In the case of n-hexadecane, some mixed solvents were also used and their compositions are shown in Table II. Freezing point data were plotted in the same manner as that of the alkanes in Isopar-M. Some of the n-hexadecane data for single solvents are shown in Figure 2. It is seen in the figure that the straight lines plotted fit the data fairly well for these four plots and this was also true for the other solutions. The solvent effect experimental data (T_m and X) were also treated by linear regression and the derived freezing point data are shown in Table III. For each of the three solutes, the solvents are listed in order of increasing ΔH_m. Literature data (13, 14) for the pure solutes are included in the table for comparison. An examination of Figure 2 and Table III shows considerable variation in the derived data for each of the solutes in the different solvents. When a solid dissolves in a liquid and an ideal solution is formed, the process may be considered equivalent to melting of the pure solute at the lowered temperature at which solution is taking place, and the ideal solubility equation implies this concept (9-12). From the ideal solubility equation (or from the solubility plots in Figures 1 and 2), it follows that relative solubility bears an inverse relationship with T_m. At a given concentration, for a relatively good solvent, solution (melting) will take place at a lower temperature than that of a relatively poorer solvent. Similarly, at a given temperature, it can be shown that solubility increases with decreasing ΔH_m for systems which obey the ideal solubility equation. In general, both $T_{m,o}$ and ΔH_m are approximate measures of relative solubility. For example, in Figure 2, it is seen that decalin (the lowest curve in the figure) is a relatively better solvent for n-hexadecane than secondary butyl benzene (the upper curve). The data in Table III also illustrate this concept. For C_{14}, in the three solvents shown in the table, n-heptane and Isopar-M are good solvents, and secondary butyl benzene, an aromatic compound, the poorest. The $T_{m,o}$ for C_{14} in Isopar-M (280°K) is the same as that of the literature value for the pure C_{14} (279°K) within experimental error. For C_{16} in individual solvents, n-heptane, decalin and Isopar-M appear to be relatively good solvents, and secondary butyl benzene the poorest. The $T_{m,o}$ values derived for decalin (289°K) and Isopar-M (290°K) solutions are the same as that of pure C_{16} within experimental error, but the n-heptane result (295°K) seems to be high. For C_{16} in mixed solvents, Solutions A, B and C are relatively good solvents, and Solution G the poorest. As seen in Table II, Solutions A, B and C consist chiefly of Isopar-M or Isopar-M and decalin which were shown above to be relatively good solvents for C_{16}. Again, the aromatic (Solution G) was the poorest. For naphthalene, as might be expected, Table III shows that secondary butyl benzene is a better solvent than Isopar-M. The $T_{m,o}$ derived from the secondary butyl benzene solutions (374°K), however, is much higher than that of pure naphthalene (354°K). The naphthalene data are limited, however, to only two solvents at a limited number of concentrations.

Tertiary Solutions

In order to observe possible interaction between n-alkanes in a common solvent and its effect on freezing point, solutions of n-C_{13} and n-C_{16} in Isopar-M were prepared at several concentrations. Standard freezing point plots of $1/T_m$ vs. Log n-C_{13} at several constant C_{16} concentrations are shown in Figure 3. The 0% C_{16} line in the graph is the curve for C_{13} in Isopar-M from Figure 1. It is seen in the figure that the 0.17% C_{16} data points fall on a parallel straight line, but at somewhat lower temperatures than that of the pure C_{13} line. However, a change is observed for higher C_{16} concentrations. The 0.42% C_{16} curve consists of two lines of opposite slopes. The section of the curve above about 3% C_{13} falls on the 0.17% C_{16} line. The 0.84% and 1.69% C_{16} data follow the pattern of the 0.42% C_{16} curve but with decreasing slopes. The 4.25% C_{16} line is horizontal, showing that changes in C_{13} concentration have no effect, and that the C_{16} has "taken over" the control of freezing point.

Two interesting observations were noted in Figure 3. First, for C_{16} concentrations of 0.42, 0.84, and 1.69% C_{16}, addition of C_{13} at the lower C_{13} concentrations causes a reduction of freezing point. The second observation, which was unexpected, is that certain combinations of C_{13} and C_{16} in Isopar-M freeze at lower temperatures than that of the same concentration of either alkane alone in the same Isopar-M base stock. For example, the freezing point of 1.04% C_{13} and 0.17% C_{16} in Isopar-M was 207°K, whereas the freezing point of 1.04% C_{13} (C_{16} = 0) was 209°K and that of 0.17% C_{16} (C_{13} = 0) was 225°K. A similar solution of 3.11% C_{13} + 0.42% C_{16} froze at 218°K, whereas the freezing points of the single alkanes in Isopar-M were 221°K and 233°K respectively for 3.11% C_{13} and 0.42% C_{16}.

The data in Figure 3 suggest that there has been interaction between the C_{13} and C_{16} in their mutual influence on the freezing points in Isopar-M solutions.

The freezing point-concentration plots for C_{13} and C_{16} in Isopar-M (Figure 1) show relatively close adherence to the ideal solubility equation suggesting a minimum of interaction between the individual solutes and solvent for either alkane. But, when together in the same solution, their mutual behavior is unexpected. The mutual solubility of two compounds is a qualitative measure of the extent of the interaction between their molecules, varying from simple departure from ideal behavior to actual compound formation between the two substances (12). In some cases, it is possible to explain deviations from ideality. Most commonly, the explanation is based on association to form dimers or trimers; compound formation between solute and solvent; or possibly dissocation of the solute to form two or more molecules (11). The last of these possible explanations (dissociation), however, would not be expected to apply to solutions of alkanes in hydrocarbon solvents. Another possible explanation is that the two alkanes form a eutectic type mixture. In the case of the C_{13}-C_{16} in Isopar-M behavior, this is now under investigation. It is hoped that by isolating the crystals which form during freezing, and identifying them, an explanation of this behavior might be forthcoming. This work is still in progress.

SUMMARY AND CONCLUSIONS

A study was made of the effect of composition on the freezing points of model hydrocarbon jet fuel type mixtures. Solutions of higher n-alkanes (C_{12} - C_{17}) in several solvents were emphasized. Freezing points (T_m) of solutions of single alkanes were found to conform with the Van't Hoff ideal solubility equation. From the slopes and intercepts of plots of concentration (Ln X) vs $1/T_m$, heats (ΔH_m) and entropies (ΔS_m) of fusion, and extrapolated freezing points of pure alkanes ($T_{m,o}$) were derived. For an isoparaffinic base solvent (Isopar-M), the derived $T_{m,o}$ values were in good agreement with the literature values for the pure alkanes. For ΔH_m and ΔS_m, only the even carbon numbered alkanes exhibited values similar to literature data for the pure compounds. This alternating behavior for the n-alkanes series has been observed for melting point and other properties of the pure compounds. For alkanes in other solvents, considerable solubility effect was noticed. For C_{14} and C_{16}, decalin and Isopar-M were found to be relatively good solvents but aromatic compounds, such as butyl benzenes, were relatively poor. For naphthalene, butyl benzene was a better solvent than Isopar-M. For mixtures of C_{13} and C_{16} in Isopar-M, significant changes or reversals of slope were observed for 1/T plotted against Ln X (C_{13} concentration) at various C_{16} concentrations, and this suggested interaction between the two alkane solutes. C_{16} had the predominant effect in C_{13} + C_{16} solutions in Isopar-M. Above about 4% C_{16}, changes in C_{13} concentration had no observable effect.

REFERENCES

1. Dimitroff, E., Gray, Jr., J. T., Meckel, N. T., and Quillian, Jr., R. D., 7th World Petroleum Congress, Mexico City, April 1967, Individual Paper No. 47.

2. Dimitroff, E. and Dietzman, H. E., American Chemical Society, Petroleum Division, Preprints, 14, B-132 (1969).

3. Petrovic, K. and Vitorovic, D., J. Inst. Pet. 59, 20 (1973).

4. Antoine, A. C., "Evaluation of the Application of Some Gas Chromatographic Methods for the Determination of Properties of Synthetic Fuels," NASA Technical Memorandum 79035, November 1978.

5. Solash, J., Hazlett, R. N., Hall, J. M. and Nowack, C. J., Fuel, 57, 521 (1978).

6. American Society for Testing and Materials, Compilation of ASTM Standard Definitions, 4th Ed, 1979.

7. American Society for Testing and Materials, "Freezing Point of Aviation Fuels," ASTM D 2386-67.

8. Humble Oil and Refining Co., Isopar-M, Data Sheet DG-1P, 1968.

9. Cines, M. R., "Solid-Liquid Equilibria of Hydrocarbons," Chap. 8, Physical Chemistry of the Hydrocarbons, A. Farkas, Ed., Academic Press, New York, 1950, pp. 315-362.

10. Williams, A. G., "An Introduction to Non-Electrolyte Solutions," Wiley, New York 1967.

11. Skau, E. L. and Wakeham, H., "Determination of Melting and Freezing Temperatures," Chap. III, Physical Methods of Organic Chemistry, Techniques of Organic Chemistry, A. Weissberger, Ed., Vol. I, Part I., Interscience, New York, 1949, pp. 49-105.

12. Vold, R. D. and Vold, M. J., "Determination of Solubility," Chap. VII, Physical Methods of Organic Chemistry, Techniques of Organic Chemistry, A. Weissberger, Ed., Vol. I, Part I, Interscience, New York 1949, pp. 297-308.

13. Rossini, F., Pitzer, K. S., Arnett, R. L., Braun, R. M. and Pimentel, G. C., "Selected Values of Physical and Thermodynamic Properties of Hydrocarbons and Related Compounds," Amer. Petrol. Instit. Research Project 44, Carnegie Press, Carnegie Inst. of Technol., Pittsburgh, 1953.

14. American Chemical Society, "Physical Properties of Chemical Compounds," Volumes I and II, Advances in Chemistry Series #15 and 22, Amer. Chem. Soc., Washington, D. C. 1955, 1959.

Table I - Freezing Point Data - n-Alkanes in Isopar-M

	Heat of Fusion ΔH_m (Kcal/Mole)		Entropy of Fusion ΔS_m (Cal/Mol-deg.)		Freezing Point* $T_{m,o}$ (°K)	
n-Alkane	Exp.	Lit.	Exp.	Lit.	Exp.	Lit.
C-12	8.8	8.80	33.1	33.4	266	264
C-13	8.9	6.81	33.4	25.4	267	268
C-14	10.5	10.77	37.3	38.6	280	279
C-15	11.4	8.27	40.5	29.2	281	283
C-16	12.7	12.75	43.7	43.8	291	291
C-17	13.2	9.68	44.6	32.8	296	295

* - Extrapolated to 100%

Table II - Composition of Mixed Solvent (% w/w)

Solution	Isopar-M	Decalin	Tetralin	Butyl Benzene (normal)	Butyl Benzene (secondary)	Butyl Benzene (tertiary)
A	40	40	-	-	20	-
B	40	40	20	-	-	-
C	80	-	20	-	-	-
D	80	-	-	-	20	-
E	80	-	-	6.7	6.7	6.7
F	50	25	-	-	-	25
G	-	-	-	33.3	33.3	33.3

Table III - Freezing Point Data - Solvent Effect

Solute	Solvent	Heat of Fusion, ΔH_m (Kcal/Mole)	Entropy of Fusion, ΔS_m (Cal/Mole-Deg)	Freezing Point* $T_{m,o}$ (°K)
n-$C_{14}H_{30}$	n-C_7H_{16}	9.3	32.8	283
"	Isopar-M	10.5	37.3	280
"	sec-Butyl Benzene	11.3	39.0	291
"	(Liter.)	10.77	38.6	279
n-$C_{16}H_{34}$	n-C_7H_{16}	11.2	37.9	295
"	Decalin	11.9	41.3	289
"	Isopar-M	12.7	43.7	291
"	sec-Butyl Benzene	14.3	47.8	300
"	(Liter.)	12.75	43.8	291
"	Solution A	12.0	41.2	291
"	" B	12.4	42.6	290
"	" C	12.4	42.4	292
"	" D	12.6	42.8	294
"	" E	12.7	43.1	294
"	" F	12.7	43.4	293
"	" G	13.3	44.7	298
Naphthalene	sec-Butyl Benzene	3.9	10.4	374
"	Isopar-M	4.7	11.4	413
"	(Liter.)	4.32	12.21	354

* - Extrapolated to 100%

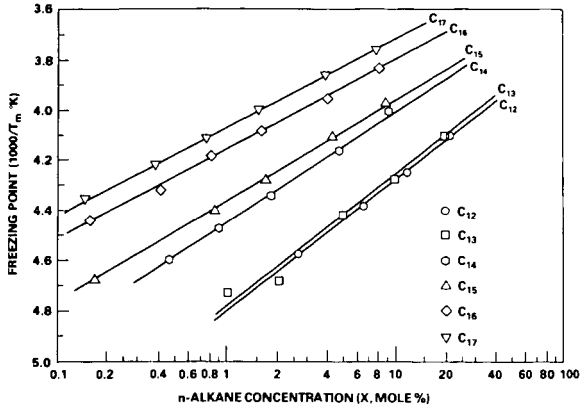

Figure 1 — Freezing Point vs Concentration — *n*-Alkanes in Isopar-M

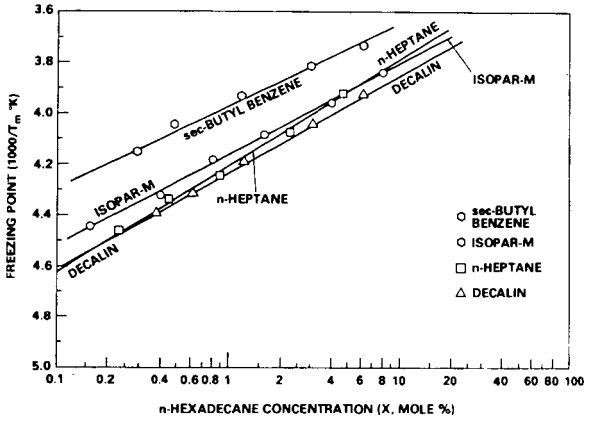

Figure 2 — Freezing Point vs Concentration — *n*-Hexadecane in Several Solvents

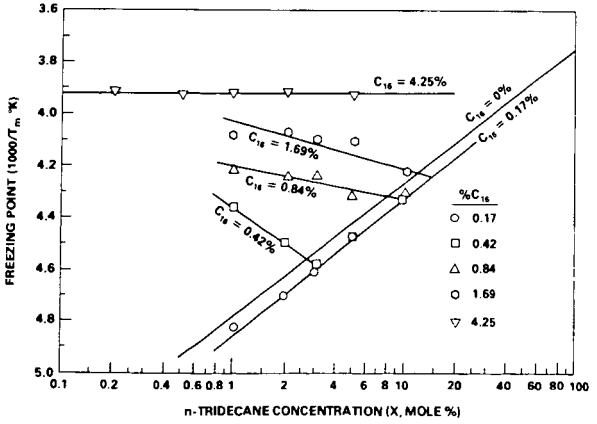

Figure 3 — Freezing Point vs *n*-Tridecane Concentration — *n*-Tridecane + *n*-Hexadecane in Isopar-M

Low-Rank Coals -- A Resource Not Fully Exploited

Irving Wender, Chemical and Petroleum
Engineering Department, University
of Pittsburgh, Pittsburgh, Pa. 15261

Total recoverable reserves of low-rank coals (subbituminous and lignite) are estimated in the hundreds of billions of tons. Almost all of this resource is located west of the Mississippi. Although increasing amounts of these coals are being used for utility purposes, less than 5% is cleaned prior to burning; probably larger amounts should be cleaned. The fact that these coals are not caking coals makes them suitable for use in certain gasifiers and the first plants for the conversion of coal to synthetic fuels will likely arise in the west. Historically coal science has largely been confined to the study of bituminous coals and there are several so-called models of 82-83% carbon coals. The structures of low-rank coals, however, remains largely a mystery. The constitution of low-rank coals, including oxygen functionality, and the effects of their mineral and moisture contents on reactivity and end use will be discussed.